





RESEARCH ARTICLE

Mapping the vocal circuitry of Alston's singing mouse with pseudorabies virus

Da-Jiang Zheng¹  | Daniel E. Okobi Jr²  | Ryan Shu¹ | Rania Agrawal¹ |
Samantha K. Smith¹  | Michael A. Long³  | Steven M. Phelps¹ 

¹Department of Integrative Biology, The University of Texas at Austin, Austin, Texas, USA

²Department of Neurology, University of California Los Angeles, Los Angeles, California, USA

³NYU Neuroscience Institute and Department of Otolaryngology, Langone Medical Center, New York University, New York City, New York, USA

Correspondence

Da-Jiang Zheng, Repair Biotechnologies, 841 E Fayette St, Syracuse, NY, 13210, USA
Email: da.jiang.zheng2@gmail.com

Funding information

Center for Neuroanatomy and Neurotropic Viruses (CNNV), Grant/Award Numbers: NIH P40 OD010996, NIH 5R01NS113071, NSF IOS-1457350

Abstract

Vocalizations are often elaborate, rhythmically structured behaviors. Vocal motor patterns require close coordination of neural circuits governing the muscles of the larynx, jaw, and respiratory system. In the elaborate vocalization of Alston's singing mouse (*Scotinomys teguina*) each note of its rapid, frequency-modulated trill is accompanied by equally rapid modulation of breath and gape. To elucidate the neural circuitry underlying this behavior, we introduced the polysynaptic retrograde neuronal tracer pseudorabies virus (PRV) into the cricothyroid and digastricus muscles, which control frequency modulation and jaw opening, respectively. Each virus singly labels ipsilateral motoneurons (nucleus ambiguus for cricothyroid, and motor trigeminal nucleus for digastricus). We find that the two isogenic viruses heavily and bilaterally colabel neurons in the gigantocellular reticular formation, a putative central pattern generator. The viruses also show strong colabeling in compartments of the midbrain including the ventrolateral periaqueductal gray and the parabrachial nucleus, two structures strongly implicated in vocalizations. In the forebrain, regions important to social cognition and energy balance both exhibit extensive colabeling. This includes the paraventricular and arcuate nuclei of the hypothalamus, the lateral hypothalamus, preoptic area, extended amygdala, central amygdala, and the bed nucleus of the stria terminalis. Finally, we find doubly labeled neurons in M1 motor cortex previously described as laryngeal, as well as in the prelimbic cortex, which indicate these cortical regions play a role in vocal production. The progress of both viruses is broadly consistent with vertebrate-general patterns of vocal circuitry, as well as with circuit models derived from primate literature.

KEYWORDS

PRV, *Scotinomys teguina*, singing mice, vocalization

1 | INTRODUCTION

Animal displays are among the most diverse and dramatic behaviors in the natural world, and their roles in courtship, aggression, and other contexts have long been the subject of behavioral studies

(Cummings & Endler, 2018). Displays also make excellent foci for neurobiological research (Fusani et al., 2014; Remage-Healey et al., 2008). Their motor patterns are complex and require the precise coordination of many muscles, but they are often highly stereotyped. Moreover, tuning a display to its ecological context requires not only

the integrated control of muscles but also the modulation of display by hormonal states and complex social cues (Schlinger et al., 2018). Identifying the neural circuits that coordinate displays can enable insights into the diversity of complex behaviors and their decision mechanisms.

Among the many forms of display, perhaps none is more widespread or well-studied than vocalization (Barkan & Zornik, 2020; Zhang & Ghazanfar, 2020). Phylogenetic studies reveal that vocalization is common and arose only a few times during vertebrate evolution (Z. Chen & Wiens, 2020). Vertebrate vocalizations function in courtship, aggression, individual identification, parental care, and many other contexts (Suthers et al., 2004). Adaptive vocalization is often sensitive to internal states like reproductive status or body condition, as well as to external cues like the immediate social environment (Gentner & Margoliash, 2006; Yamaguchi & Kelley, 2003).

Classic studies on vocal mechanisms in primates have combined tract-tracing, electrophysiology, pharmacological manipulation, and other methods to identify substrates of vocal behavior, from limbic cortex to the spinal cord (Jürgens, 2009). A smaller body of work builds and extends this into model rodent species, such as the lab mouse and lab rat (Bennett et al., 2019; Tschida et al., 2019). Overall, this literature suggests some surprising commonalities to rodent and primate vocal circuitry. Among songbirds, for example, the emphasis has often been on forebrain circuits for song learning (Brainard & Doupe, 2013) and production (Fee et al., 2004). In African clawed frogs and in the plainfin midshipman fish, vocal work has focused on motor mechanisms at the level of the brainstem and lower, and on their coordination by limbic structures in the hypothalamus and amygdala (Goodson & Bass, 2002; Hall et al., 2013). Together, the results suggest features of neural organization that may be shared across vocal vertebrates (Kelley et al., 2020). Here, we seek to elucidate the vocal circuitry in a novel mammalian model, Alston's singing mouse (*Scotinomys teguina*), by performing viral tract-tracing targeting specific vocal muscles. We compare these findings to reports in mammals and other tetrapods.

Alston's singing mice are small muroid rodents in the family Cricetidae, which make long, relatively loud vocalizations in the range of human hearing (Campbell et al., 2010; Hooper & Carleton, 1976; Miller & Engstrom, 2007). During vocalization, animals assume an upright posture, open their mouths, and angle their snouts upward (Banerjee et al., 2019; Hooper & Carleton, 1976; Riede & Pasch, 2020). Each song consists of a series of frequency-modulated notes (Campbell et al., 2010). Each note requires opening the mouth and making a short exhalation that accompanies vocalization (Okobi et al., 2019; Pasch et al., 2011a). The vocalization is highly stereotyped, with each song consisting of frequency-modulated notes that lengthen regularly as the song progresses (Campbell et al., 2010). The song is used for female attraction (Fernández-Vargas et al., 2011), male–male aggression (Pasch et al., 2011b), and species recognition (Pasch et al., 2013). It is modulated by reproductive state, stress reactivity, and energy balance (Burkhard et al., 2018; Crino et al., 2010; Giglio & Phelps, 2020; Pasch et al., 2011a). Like many displays, singing would seem to require a network of brain regions that integrate diverse cues and translate them

into adaptive, rhythmic motor patterns. Although the singing mouse is a compelling species for behavioral study, we know relatively little about the neural mechanisms of *Scotinomys* vocalization.

To quickly elucidate the vocal circuits of *S. teguina*, we employed the pseudorabies virus bartha (PRV-Bartha; Card & Enquist, 2014). PRV-Bartha is a strain of alpha-herpes virus that has been attenuated for the use of retrograde trans-synaptic transport in mammalian neurons (Card & Enquist, 2014; Pickard et al., 2002). This trans-synaptic spread enables us to examine multiple candidate brain structures. In addition, the time of arrival of the virus in a specific region allows a preliminary estimation of the network topology (Banfield et al., 2003). Lastly, the availability of multiple isogenic strains of PRV-Bartha allows dual labeling of neurons that shape the activity of different end-organs (Hogue et al., 2018). Although the dual isogenic PRV approach has been used extensively to examine the control of feeding, homeostasis, and sympathetic function (Doslikova et al., 2019; Pérez et al., 2011; Stanley et al., 2010; Wee et al., 2019; Wiedmann et al., 2017), to our knowledge it has not been used in the context of vocalization.

In the current study, we use a dual-label approach to infect two distinct muscles that play essential roles in the vocalizations of singing mice. The first target is the cricothyroid muscle, an intrinsic muscle of the larynx important to frequency modulation (Riede, 2013). The second target is the digastricus muscle, which opens the jaw. Because these two muscles must be coordinated to produce the regularly repeated notes of a *Scotinomys* song, we reasoned that identifying neurons that were double labeled would reveal circuits involved in vocalization. To do so, we injected one PRV-Bartha strain expressing green fluorescent protein (GFP), and another expressing red fluorescent protein (RFP) into either the jaw or the larynx. The two injections were ipsilateral and of equal viral titers. We describe how viruses injected into each muscle arrive into regions of the vocal circuit over time, and we quantify the number of cells each virus infects as well as the number of coinfecting cells. Finally, we compare the order of arrival of these viruses to known network topologies in other species. Together, these data allow us to quickly characterize the vocal circuitry of a novel model for mammalian vocalization, Alston's singing mouse.

2 | METHODS

2.1 | Animals

We used 16 male *S. teguina* outbred from a wild population caught near Quetzal Education Research Center in San Gerardo de Dota, Costa Rica. We have reported housing and husbandry previously (Zheng et al., 2021). All animal protocols were approved by the IACUC committee at The University of Texas at Austin in accordance with the National Institute of Health Guide for the Care and Use of Laboratory Animals. *S. teguina* weighed 15.2 ± 1.5 g and were at 143 ± 28 days of age at the time of viral inoculation. Animals were housed in a biosafety level 2 facility.

2.2 | Pseudorabies virus

We obtained USDA Aphis approval (Permit #135766) allowing for interstate shipment of PRV-Bartha from Princeton University to The University of Texas at Austin and from UT Austin's Institutional Biosafety Committee to acquire and employ the virus in our facility. We received two isogenic recombinants of the Bartha strain of PRV from the Center for Neuroanatomy and Neurotropic Viruses. PRV-152 expressing enhanced GFP (eGFP; titer: 2.45×10^9 pfu/ml) and PRV-614 expressing monomeric RFP1 (mRFP1; titer: 1.55×10^9 pfu/ml). Upon receipt of the stocks, the viruses were aliquoted at 20 μ l/cryovial in a biosafety cabinet, flash frozen, and stored in a locked -80°C freezer. On the day of surgery, individual cryovials were placed in a dedicated freezing container (Nunc, NY, USA) and thawed immediately before injection. Excess virus was inactivated by 10% bleach at a ratio of 10:1 and disposed in biosafety waste.

Subjects were anesthetized using isoflurane (5% induction, 2.5% maintenance) mixed with oxygen at a flow rate of 1 ml/min. A dedicated anesthetist monitored and recorded the anesthesia plane during surgery. The animal was placed on a Kopf 900 stereotax on top of an infrared heating pad (Kent Scientific, CT, USA). The stereotax fitted with a 923-B mouse gas anesthesia head holder (Kopf Instruments, CA, USA) allowing for rotation along the vertical axis. Once rotated, a small amount of depilatory cream, Nair, was applied in the jaw and throat area for less than 1 min. The area was then sterilized with an alternating application of providone-iodine and 70% ethanol. Analgesics including carprofen, slow-releasing buprenorphine, and lidocaine were applied.

Given the difference in titer between the two strains, we adjusted injection volumes to deliver an approximately equal titer of each virus (500 nl PRV 154, 700 nl PRV-614, $\sim 1.1\text{--}1.2 \times 10^3$ pfu). Viruses were always given ipsilaterally. The virus assigned to each muscle, and the side of the body targeted (left or right) was randomized and counter-balanced.

We first targeted the cricothyroid muscle, which was exposed through a 1 cm incision, accessing the sternohyoid muscle. A 0.5 cm incision was made to expose the larynx and its internal muscles. Overall, our cricothyroid injection approach was similar to a previously reported surgical procedure (Arriaga et al., 2015). We used a nanoliter injector (Nanoject III; Drummond, PA, USA) to deliver a predetermined amount of the PRV into the muscle. The injector was fitted with a pulled (P-2000; Sutter Instruments, CA, USA) Wiretrol I calibrated micropipette (Drummond) and forged to a tip of 20 μm I.D (Narishige, NY, USA). We injected 100 nl boluses at a rate of 3 nl per second separated by 1 min. After the cricothyroid injection, we would dispose the pipette in bleach and prepare a second pipette for the other PRV strain into the digastricus. Another 1 cm incision was made in the jaw area of the subject, exposing the posterior and anterior digastricus. We injected unilaterally into the anterior digastricus at the same rate as the cricothyroid injection. After delivering the virus, the muscles were dried with a sterile cotton swab and the skin flap was glued together with Vetbond (3 M, MN, USA). Animals were housed individually and monitored every 12 h.

The cricothyroid is a small interior muscle and required some development of surgical technique. We first used Evans blue in the absence of virus to inject the cricothyroid and later imaged laryngeal sections to confirm placement. In these sections, we saw evidence of Evans blue in the cricothyroid (including blue pigment and red fluorescence, a known consequence of the dye binding to myoglobin-damaged muscle), but no evidence of penetration of other muscles. During the surgeries in the current study, PRV was coinjected with Evans blue, allowing us to visualize any viral efflux at the time of injection. We did not see viral efflux at any volumes used, nor did we see any staining of adjacent muscles. The cricothyroid surgery displaces the sternohyoid muscle so that the cricothyroid is directly exposed—that is, the needle containing PRV does not penetrate any other muscle. We thus believe it is unlikely that infection of other motor neurons confounds our results.

Previous results have demonstrated that double viral injections with these strains have similar infection kinetics as single injections (Banfield et al., 2003; Hettigoda et al., 2015; Hogue et al., 2018; Jovanovic et al., 2010; Stanley et al., 2010; Wee et al., 2019). In pilot work, we performed unilateral injections targeting the cricothyroid and digastricus muscle separately with the animals sacrificed at 48 and 60 h postinjection (hpi). We observed very little infection in subjects infected for less than 60 h. Conversely, subjects were moribund at 96 hpi. We first sought to characterize the time-course and extent of infection using six animals at three time points (72, 84, and 96 hpi; $n = 2$ per time point). At 72 h, only a few structures in the brainstem and spinal cord were labeled, so we injected a larger group of 10 animals at two time points (84 and 96 hpi, $n = 5$ per time point).

To quantify patterns of labeling and colabeling, we selected a subset of brain regions expressing markers for one or both viruses, and spanning a full range of neuroanatomical levels—including regions of the brainstem, midbrain, hypothalamus, amygdala, and neocortex. We quantified single and double labeling in our final cohort of 96 h subjects ($n = 5$) and report qualitative findings for the remainder of our samples. Sample sizes, targeted tissues, and virus–muscle assignments are summarized in Table 1.

2.3 | Tissue dissections and cryosectioning

At set time points (Table 1), animals were euthanized by isoflurane to effect, and then transcardially perfused with a peristaltic pump (Cole-Parmer, IL, USA), first with cold 1X PBS (Thermo Fisher Scientific, MA, USA) and then cold 4% paraformaldehyde (EMS, PA, USA) in 1X PBS. Brains were removed, postfixed in 4% paraformaldehyde for 24 h at 4°C , and then cryoprotected in 15% followed by 30% sucrose. After cryoprotection, brains were frozen on powdered dry ice and stored in a -80°C freezer until sectioning. We collected alternating series at 30 μm with an HM550 cryostat (Thermo Fisher Scientific) beginning just caudal to the nucleus ambiguus, corresponding to approximately -7.50 mm with reference to Franklin & Paxinos, (2007), and extending rostrally until appearance of the accessory olfactory nucleus. For qualitative study, individual sections were placed in a cryoprotectant (de

TABLE 1 An overview of pseudorabies virus (PRV) type and injection strategy, including survival times included in this study

Subject ID	PRV 152 Inj	PRV 614 inj	Time point
1	R. Cricothyroid	R. Digastricus	72 hpi
2	R. Digastricus	R. Cricothyroid	72 hpi
3	R. Cricothyroid	R. Digastricus	84 hpi
4	R. Digastricus	R. Cricothyroid	84 hpi
5	R. Cricothyroid	R. Digastricus	96 hpi
6	R. Digastricus	R. Cricothyroid	96 hpi
7	R. Cricothyroid	R. Digastricus	84 hpi
8	R. Digastricus	R. Cricothyroid	84 hpi
9	L. Cricothyroid	L. Digastricus	84 hpi
10	L. Digastricus	L. Cricothyroid	84 hpi
11	R. Cricothyroid	R. Digastricus	84 hpi
12	R. Cricothyroid	R. Digastricus	96 hpi*
13	R. Digastricus	R. Cricothyroid	96 hpi*
14	L. Cricothyroid	L. Digastricus	96 hpi*
15	L. Digastricus	L. Cricothyroid	96 hpi*
16	R. Cricothyroid	R. Digastricus	96 hpi*

Abbreviations: hpi, hours postinjection; inj, injection; L, left; R, right.
 *denotes subject used in quantitative study.

Olmos solution) and stored at -20°C until immunofluorescence. For our quantitative study, individual sections were mounted on a Superfrost Plus slide (Thermo Fisher Scientific) and stored at -80°C until immunofluorescence. No individual section was exposed to more than one freeze-thaw cycle. We noticed no qualitative difference in brain areas infected between the sections stored in wells and those mounted on slides.

2.4 | Immunofluorescence

All antibodies, ratios, RRIDs, and prior publications using the antibodies are reported in Table 2. One of the two series collected was used for multiplex immunofluorescence of eGFP and mRFP signal. In our transition from our time course analysis to our focal sample, we changed the RFP antibody to allow us to triple label sections with a specific androgen receptor antibody PG21 (Prins et al., 1991)—data we have yet to compile, and that are not part of our current study. This antibody change had no discernible effect on our labeling patterns.

We labeled the most of the rostral-caudal axis of the *S. teguina* brain. We first washed in 1X PBS for three times and then incubated in a blocking solution with 10% normal serum, 0.3% Triton X, and 1X PBS for 1 h. Sections were rinsed again with 1X PBS three times and then incubated in 5% normal serum, 0.3 Triton X, 1X PBS, with the primary antibody (Table 2) for 24 h at room temperature. Sections were then rinsed again three times in 1X PBS and then incubated in corresponding

secondary antibodies for 2 h at room temperature (Table 2). Slides were then covered and stored at 4°C under dark conditions until microscopy.

2.5 | Microscopy and cell counting

Imaging was performed at the Center for Biomedical Research Support at the University of Texas at Austin with a W1 Yokogawa spinning disk confocal microscope (Nikon, NY, USA). Excitation laser power was optimized for 488, 561, and 640 nm channels, and a Plan Fluor DLL Ph1 10X/0.3NA objective was used to collect all images. Respective laser power was kept consistent through all imaging of tissue samples. For tiling of large images, a scan large-image macro was used with a 20% overlap and blending option. Images collected in this fashion were used for qualitative assessment of infection.

We used both the Paxinos and Franklin third edition atlas (Franklin & Paxinos, 2007) along with the Allen Brain atlas (Lein et al., 2007) to delineate regions of interest (ROIs). ROIs reported, number of bregma levels, and the estimate bregma level according to Paxinos and Franklin are reported in Table 3. Pseudo-colored images were automatically thresholded for brightness and contrast in ImageJ, and soma were counted using the Cell Counter suite. The merged color was then split by channel and counted again for virus-specific infection. Each image was counted twice, once by the primary scorer (DJZ) and once by a naïve scorer (RA). Muscles were randomly assigned to either the RFP- or GFP-containing viruses, and these were counterbalanced across animals. For clarity, we present infections by the cricothyroid as green and digastricus as magenta and dual infections as white.

3 | RESULTS

The overall goal of our study is to explore the system of interconnected brain regions that innervate two muscles (cricothyroid and digastricus) that are involved in the stereotyped vocalizations of *S. teguina* (Figure 1a). The infection by the dual PRVs was both pervasive and specific (Figure 1b). Below, we describe a systematic survey of label originating from either the cricothyroid, the digastricus, or both. The description of labeling begins at the caudal boundary of regions that were sampled across individuals. Because there is no atlas of the singing mouse brain, we refer to “bregma levels” with respect to the *Mus musculus* atlas of Franklin and Paxinos (2007) to describe the relative position of the staining. For the subset of structures that we quantified by cell-counting, these levels are also reported in Table 3.

3.1 | Brainstem and spinal cord

Cricothyroid injection resulted in a single-labeled, ipsilateral infection in the nucleus ambiguus (Figure 2a). The nucleus was labeled at 72 h, the earliest timepoint observed for any neurons labeled with virus injected into the cricothyroid (Figure 2b,c). The infection was restricted to the rostral portion of the nucleus ambiguus, roughly coinciding with

TABLE 2 List of antibodies used in this study

Target	Host	Dilution	Source	Catalog number	RRID	References
Primary antibodies						
GFP	Chicken	1:1000	Abcam	Ab13970	AB_300798	Schneider et al. (2019)
RFP	Rabbit	1:500	Abcam	Ab62341	AB_945213	Yao et al. (2018)
RFP	Goat	1:500	Rockland	200-101-379	AB_2744552	Chen et al. (2017)
Tyrosine hydroxylase	Sheep	1:1000	Millipore	AB1542	AB_90755	Greenberg et al. (2015)
Secondary antibodies						
Chicken Alexa Fluor 488	Donkey	1:200	Jackson Immuno	703-545-155	AB_2340375	
Rabbit Alexa Fluor 594	Donkey	1:200	Thermo Fisher	A21207	AB_141637	
Goat Alexa Fluor 594	Donkey	1:200	Thermo Fisher	A11058	AB_142540	
Sheep Alexa Fluor 680	Donkey	1:200	Thermo Fisher	A21102	AB_1500713	

Abbreviations: GFP, green fluorescent protein; RFP, red fluorescent protein.

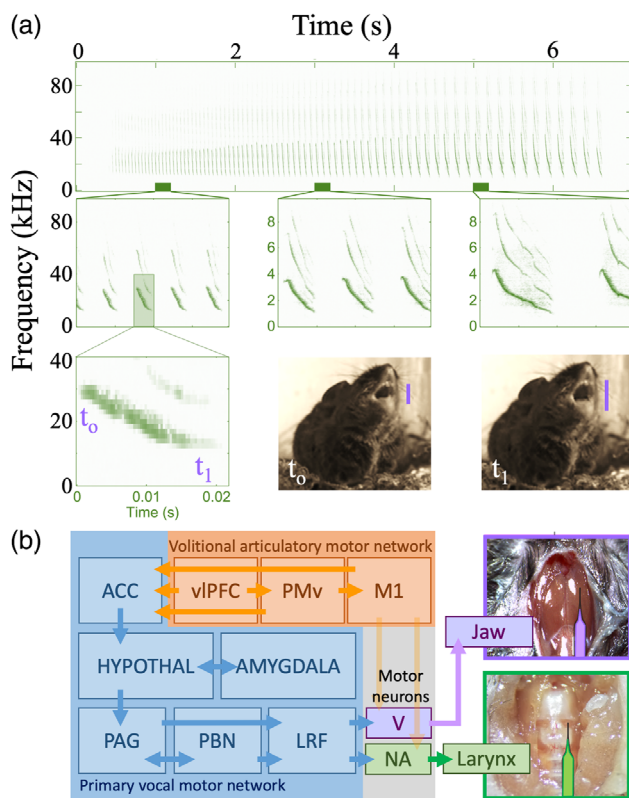


FIGURE 1 Schematic of experimental approach. (a) High-speed capture of the advertisement call behavior of *S. teguina*. Vocal gape indicated by vertical lines. Images courtesy of Dr Bret Pasch, NAU. (b) relative target positions of the muscles in this study. (c) Adaptation of schematic from Hage and Nieder (2016) as applied to this current experiment (Hage & Nieder, 2016). V, motor trigeminal nucleus; ACC, anterior cingulate cortex; HYPOTHAL, hypothalamus; LRF, lateral reticular formation; M1, primary motor cortex; NA, nucleus ambiguus; PAG, periaqueductal gray; PBN, parabrachial nucleus; PMv, ventral premotor cortex; vIPFC, ventrolateral prefrontal cortex. Note: (b) represents a simplified schematic as it does not represent an exhaustive list of projections, and some projections represented by arrows may be polysynaptic. For example, the ACC projects directly to the PAG

TABLE 3 List of regions of interest (ROIs) quantified in this study

ROI	Number of sections counted	Bilateral/unilateral	Approximate bregma ¹
DMPSP5	2	Unilateral	-6.64
AMB	5	Unilateral	-6.64
NTS	5	Bilateral	-6.64
GI	5	Bilateral	-6.64
LC	5	Bilateral	-5.68
LPB	5	Bilateral	-5.68
MPB	5	Bilateral	-5.52
DMPAG	10	Unilateral	-4.96
LPAG	10	Bilateral	-4.96
LH	5	Bilateral	-2.3
PVN	5	Unilateral	-0.82
BNST	5	Bilateral	0.02
M1	5	Unilateral	-0.10
PrL	3	Bilateral	1.94

Abbreviations: AMB, nucleus ambiguus; BNST, bed nucleus of the stria terminalis; DMPSP5, dorsomedial trigeminal nucleus; DMPAG, dorsomedial periaqueductal gray; Gi, gigantocellular reticular nucleus; LC, locus coeruleus; LH, lateral hypothalamus; LPAG, lateral periaqueductal gray; LPB, lateral parabrachial nucleus; M1, primary motor cortex; MPB, medial parabrachial nucleus; NTS, nucleus of the solitary tract; PrL, prelimbic cortex; PVN, paraventricular nucleus.

¹Approximate bregma levels are referenced from Franklin and Paxinos (2007) from where counting began rostral to caudal coronally in millimeter.

the presence of the inferior olive, which is devoid of infection. In contrast, areas surrounding the nucleus ambiguus, particularly the prebotzinger complex, were labeled by the digastricus virus at 72 h, and colabeled by both at 84 and 96 h (Figure 2a,c). By 96 h, a few double-labeled cells were present in the ipsilateral nucleus ambiguus, as well as a small number of labeled contralateral neurons (see Figure 2a,c; Table 4).

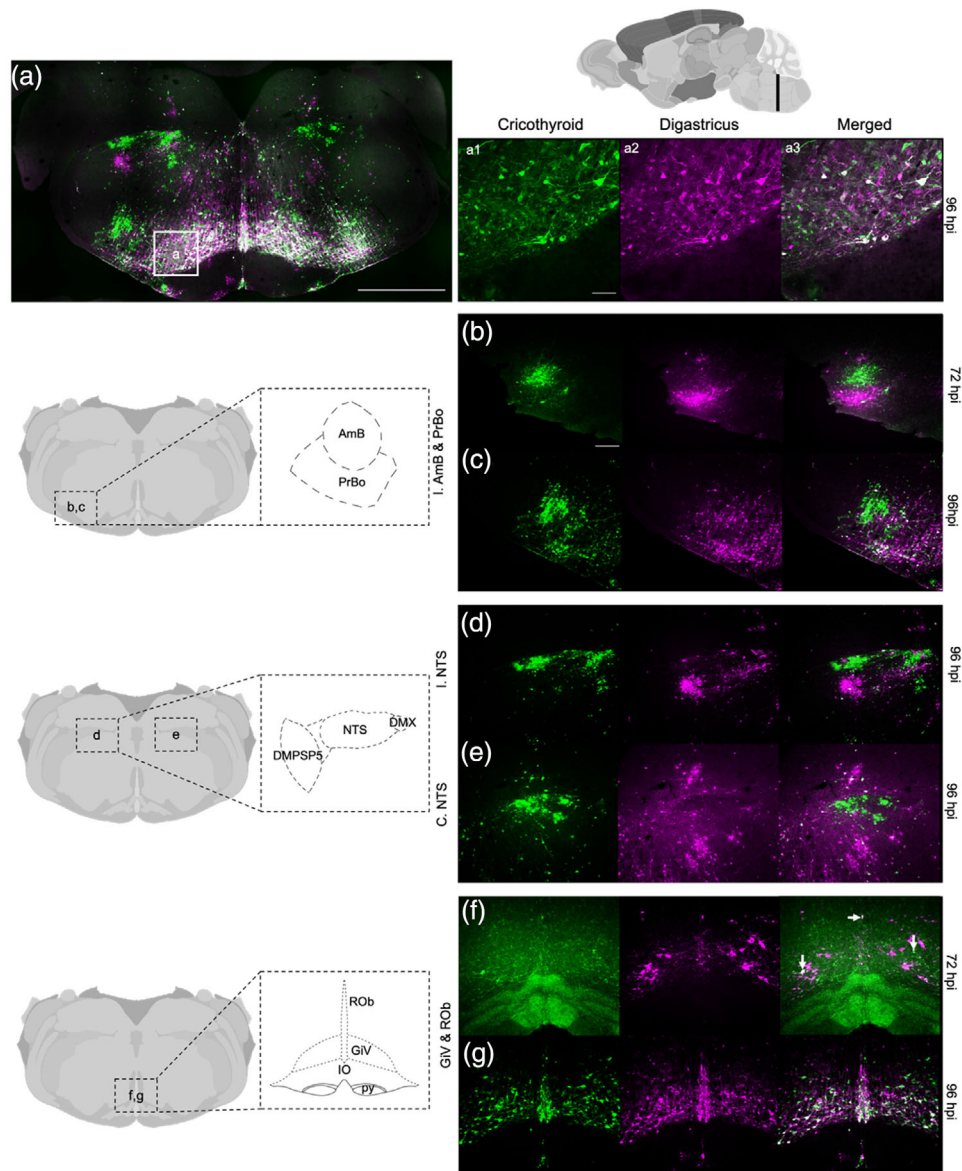


FIGURE 2 Hindbrain I. (a) Tile scan of the medulla, scale bar = 1 mm. (a), Higher magnification of colabeling, scale bar = 100 μ m. (b) Nucleus ambiguus at 72 h postinjection (hpi), scale bar = 200 μ m. (c) Nucleus ambiguus at 96 hpi. (d) Ipsilateral nucleus of the solitary tract at 96 hpi. (e) Contralateral nucleus of the solitary tract at 96 hpi. (f) Gigantocellular reticular nucleus and raphe obscurus at 72 hpi. (g) Gigantocellular reticular nucleus and raphe obscurus at 96 hpi. AmB, nucleus ambiguus; C, contralateral; DMPSP5, dorsomedial spinal trigeminal nucleus; DMX, dorsal motor nucleus of the vagus; GiV, gigantocellular reticular nucleus, ventral part; I, ipsilateral; IO, inferior olive; NTS, nucleus of the solitary tract; PrBO, prebotzinger complex; py, pyramidal tract

The nucleus of the solitary tract (NTS) became infected by both viruses at 84 h, with few double-labeled neurons (Figure 2a,d; Table 4). Cricothyroid staining is bilateral in the NTS, while the digastricus stain is ipsilateral (Figure 2d,e). The infection of the NTS is extensive, spanning from the recess of the locus coeruleus to bregma -7.50 mm (Franklin & Paxinos, 2007), the caudal limit of our sample. Adjacent to the NTS, the ipsilateral dorsomedial spinal trigeminal nucleus (DMPSP5) labels for digastricus but not cricothyroid virus (Figure 2d). The DMPSP5 infection is restricted to the rostral ~ 120 μ m of the

nucleus, reflecting previous reports of its functional heterogeneity (Iv et al., 2014).

The gigantocellular reticular nucleus (Gi) is a large, doubly labeled region (Figure 2a,f,g). Together with the lateral paragigantocellular reticular nucleus (LPGi) and the raphe obscurus (ROb), these contiguous structures begin to be double labeled at 72 hpi (Figure 2f). Unlike the nucleus ambiguus or DMPSP5, these nuclei are stained bilaterally from their first detectable infections (Figure 2g). At the equivalent of coronal sections corresponding to bregma -5.70 mm in mice

TABLE 4 Average number of pseudorabies virus (PRV)-labeled neurons projecting to each structure and colabeled

ROI	Larynx	Jaw	Colabeled
DMPSP5	6.8	32.8	2.2
AMB	52.6	7.6	4.2
C.NTS	199.4	86.8	13
I.NTS	196.6	185.4	15.4
Gi	224.6	202.6	109.8
C.LC	72.4	70.4	54.4
I.LC	79.8	76.6	55
C.LPB	28	30.4	5.4
I.LPB	37	34.4	8
C.MPB	118.4	114	66.6
I.MPB	177	181.2	109
DMPAG	209.2	198.4	45.6
C.LPAG	215.2	201	123.4
I.LPAG	210	186.2	115.4
C.LH	227	204	98.4
I.LH	248.2	236.4	116.4
PVN	134.8	119.8	41.6
C.BNST	108.8	102.6	61.2
I.BNST	159	153.6	64.8
M1	27.4	26.2	14.6
C.PrL	1.6	1	0.2
I.PrL	6.6	6.6	3.6

Abbreviations: AMB, nucleus ambiguus; BNST, bed nucleus of the stria terminalis; C., contralateral; DMPSP5, dorsomedial trigeminal nucleus; DMPAG, dorsomedial periaqueductal gray; Gi, gigantocellular reticular nucleus; I., ipsilateral; LC, locus coeruleus; LH, lateral hypothalamus; LPAG, lateral periaqueductal gray; LPB, lateral parabrachial nucleus; M1, primary motor cortex; MPB, medial parabrachial nucleus; NTS, nucleus of the solitary tract; PrL, prelimbic cortex. PVN, paraventricular nucleus; ROI, region of interest.

(Franklin & Paxinos, 2007), we observe extensive colabeling in the locus ceruleus (LC) beginning at 84 h (Figure 3a–c). To confirm the identity of the LC, we performed tyrosine hydroxylase (TH) immunolabeling on an alternate series of sections and found extensive triple labeling of TH, cricothyroid, and digastricus PRV infections (Figure 15a).

The parvicellular reticular nucleus (PCRt) is double-labeled, with the cricothyroid label emerging at 84 h and the digastricus at 96 h (Figure 3a–e). This infection may also include the adjacent intermediate reticular nucleus (IRt), but the boundaries between PCRt and IRt are not readily discernible.

As mentioned above, the gigantocellular reticular formation (Gi) extends rostrally into the plane that contains PCRt (Figure 3a,f), coincident with the beginning of the pyramidal tract and just rostral to the inferior olive, a level we interpret as Gi alpha (GiA). At this level, the Gi is contiguous with the caudal regions of the raphe magnus nucleus (RMg) at the equivalent of Franklin and Paxinos (2007) bregma -5.30 (Figure 3f).

At the level of the RMg, we note the primary motorneuron pool for the anterior digastricus, a subdivision of the motor trigeminal nucleus (5N) known as 5ADi. Beginning at 72 h, it is infected by the digastricus PRV alone. The double-labeled neurons of RMg extend past the rostral boundary of the Gi (Figure 4a). The label is ipsilateral and remains specific to the digastricus-targeted PRV through 96 h (Figure 4b,c). Outside of 5ADi, 5N is sparsely but specifically infected by the virus targeted to the digastricus (Figure 4c).

Just lateral to the paraventricular nucleus, we find another catecholaminergic site, A5 cells, are double labeled at both the 84 and 96 hpi (Figure 3d,e). At 84 h, the structure is more clearly delineated by colabeling than at 96 h (Figure 3d,e).

Lateral and ventral to the periaqueductal gray (PAG) and the aqueduct, we observe heterogeneous labeling among divisions of the parabrachial nucleus. At 84 h, double-labeled cells arise in the medial parabrachial nucleus (MBP), while the lateral portion does not show substantial infection (Figure 4f). At 96 h, the MPB is densely colabeled (Figure 4g), the LPB has both labels, but few neurons are doubly labeled.

Regions of brainstem evident at the level of the PAG, specifically the PB and the RMg, show similar patterns of double labeling and timing as observed more caudally (Figures 4 and 5), with sparse labeling at 84 h and strong labeling at 96 h. The pontine reticular nucleus (PnO) exhibits a similar pattern of infection, with sparse double label evident at 84 h, and more extensive staining at 96 hpi (Figure 5f,g).

3.2 | Midbrain

The PAG, a canonical structure in the regulation of vocalization, shows substantial heterogeneity of labeling (Figures 5–9). Unlike regions of the brainstem, there is no labeling evident at 72 h. At the caudal boundary of the PAG, where the cerebellar vermis appears in the aqueduct (Figure 5a), we see double-labeled cells appear in the lateral PAG (LPAG) and ventral lateral PAG (VLPAG) beginning at 84 hpi (Figure 5b,c). There seems to be a lack of labeling of the dorsal lateral PAG (DLPAG) altogether, and a late arrival of labeling (96 hpi) in the dorsal medial PAG (DMPAG). At 96 hpi, labeling and colabeling of the viruses are contiguous between the VLPAG and the lateral dorsal tegmentum LDTg (Figure 5c). The same pattern of labeling is evident rostrally (Figures 6–8).

At the equivalent of bregma -3.00 mm (Franklin & Paxinos, 2007), the zona incerta (ZI) exhibits digastricus label at 84 hpi and is dually labeled at 96 h (Figure 8b,c).

At the rostral end of the PAG, the p1PAG is colabeled beginning at the 96-h time point (Figure 9a,b). At this same level, the A11 dopaminergic cell group is also colabeled for cricothyroid and digastricus PRV beginning at 96 hpi (Figure 9c). The catecholaminergic identity of the putative A11 group was confirmed by TH labeling (Figure 15c); the group of TH+ and PRV-double-labeled cells seemed more expansive than reported in Franklin and Paxinos (2007).

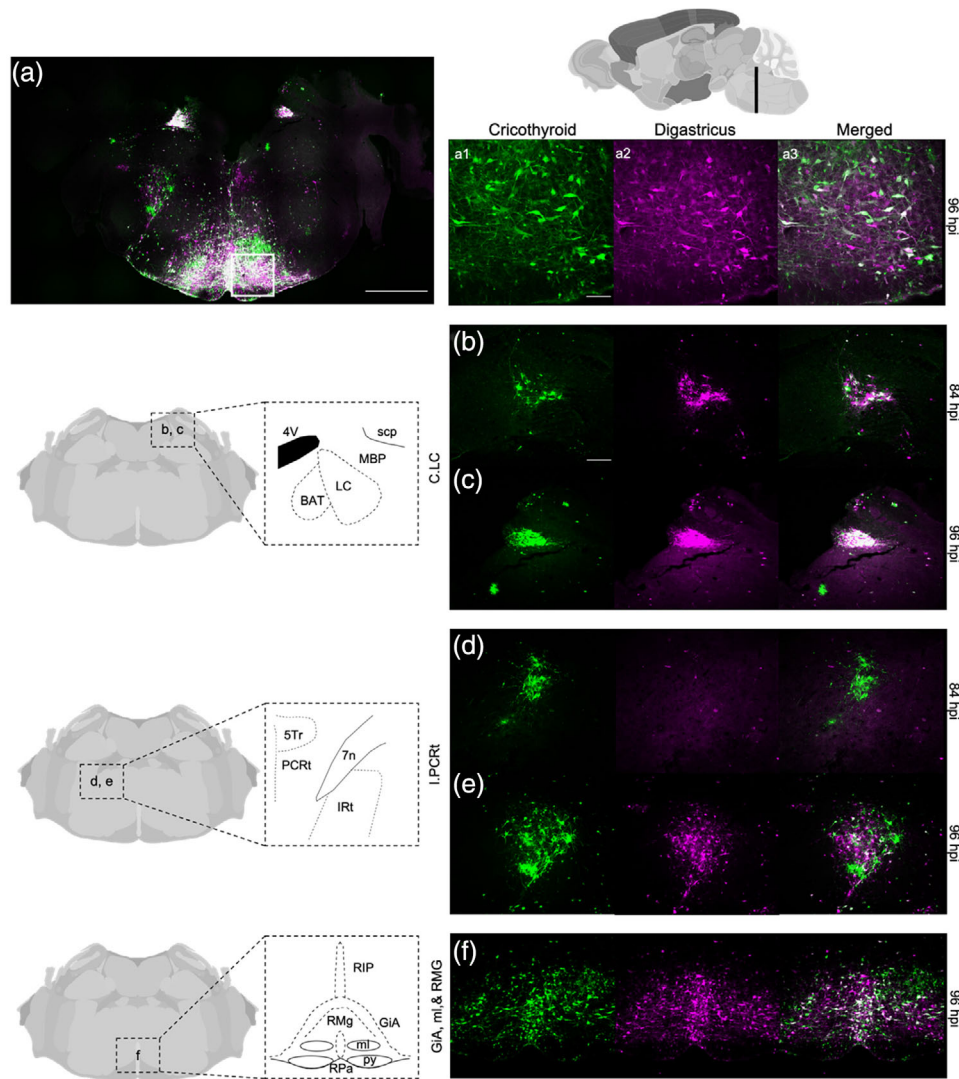


FIGURE 3 Hindbrain 2. (a) Tile scan of the pons, scale bar = 1 mm. (a) High magnification of colabeling, scale bar = 100 μ m. (b) Locus coeruleus at 84 h postinjection (hpi), scale bar = 200 μ m. (c) Locus coeruleus at 96 hpi. (d) Ipsilateral parvocellular reticular nucleus at 84 hpi. (e) Ipsilateral parvocellular reticular nucleus at 96 hpi. (f) Gigantocellular reticular nucleus, alpha part and raphe magnus nucleus at 96 hpi. 4V, fourth ventricle; 5Tr, trigeminal transition zone; 7n, facial nerve; BAT, Barrington's nucleus; C, contralateral; GiA, gigantocellular reticular nucleus, alpha part; I, ipsilateral; IRT, intermediate reticular nucleus; LC, locus coeruleus; MBP, medial parabrachial nucleus; ml, medial lemniscus; PCRT, parvocellular reticular nucleus; RIP, raphe interpositus nucleus; RMg, raphe magnus nucleus; RPa, raphe pallidus nucleus; py, pyramidal tract; scp, superior cerebellar peduncle

3.3 | Hypothalamus and amygdala

The arcuate nucleus (ARC) is colabeled by the two viruses at both 84 and 96 h (Figures 9 and 10). The colabeling was specific mostly to the lateral posterior portion with no labeling in the median eminence. At the caudal boundaries of the arcuate nucleus labeling, we also observe coinfection of the dorsomedial hypothalamus (DM) (Figure 10a,b) and the lateral hypothalamus (LH) (Figure 10c,d) at both 84 and 96 h. We note that only a small portion of the DM was labeled, and none of the ventral medial hypothalamus (VMH).

Like the ARC, LH, and parts of the DM, the paraventricular nucleus of the hypothalamus (PVN) exhibits substantial double labeling beginning at 84 hpi (Figure 10f,g). Rostral to the PVN, the medial preop-

tic area (MPOA), as well as the median preoptic area (MnPOA), are strongly colabeled beginning at 84 hpi (Figure 10h,i), and more densely at 96 hpi (Figure 10j).

The central amygdala (CeA) exhibits double labeling in its medial portion beginning at 84 hpi (Figure 11a) and expanding laterally into the remainder of the CeA at 96 hpi (Figure 11b). Similarly, medial and rostral to the CeA, the extended amygdala (EA) begins to be colabeled at 84 h (Figure 11c) although the initial label is from the digastricus inoculation. At 96 h, the EA is sparsely colabeled (Figure 11d). Lastly, in the bed nucleus of the stria terminalis (BNST), colabeling emerges at 96 hpi (Figure 11e). At 96 hpi, we observe a few double-labeled neurons in the lateral septum (not shown).

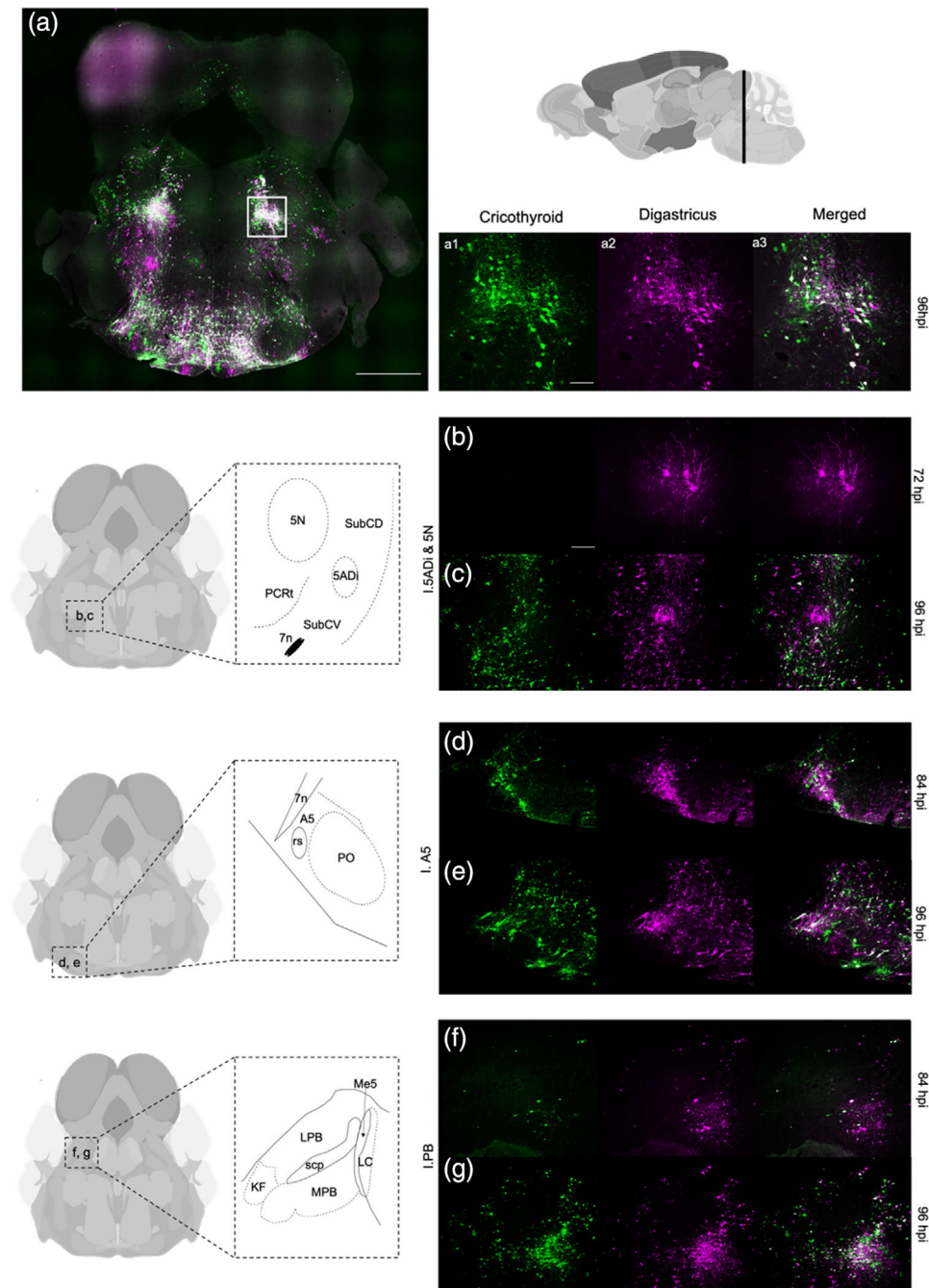


FIGURE 4 Hindbrain 3. (a) Tile scan of caudal portion of the midbrain, scale bar = 1 mm. (a), higher magnification of colabeling, scale bar = 100 μm . (b) Motor trigeminal nucleus, anterior digastric portion at 72 h scale bar = 200 μm . (c) Motor trigeminal nucleus, anterior digastric portion at 96 h. (d) Ipsilateral A5 cell population at 84 h. (e) Ipsilateral A5 cell population at 96 h. (f) Ipsilateral parabrachial nucleus at 84 h. (g) Ipsilateral parabrachial nucleus at 96 h. 5ADi, motor trigeminal nucleus, anterior digastric part; 5N, motor trigeminal nucleus. 7n, facial nerve; A5, A5 nonadrenaline cells; C, contralateral; I, ipsilateral; KF, Killiker-Fuse nucleus; LC, locus coeruleus; LPB, lateral parabrachial nucleus; Me5, mesencephalic trigeminal nucleus; MBP, medial parabrachial nucleus; PCRt, parvicellular reticular nucleus; PO, periolivary region; rs, rubrospinal tract; scp, superior cerebellar peduncle; SubCD, subcoeruleus nucleus, dorsal part; SubCV, subcoeruleus nucleus, ventral part

3.4 | Cortex

We observe PRV infection in three distinct cortical regions in the *S. teguina* brain. At the caudal portions of the midbrain where the aqueduct appears, the ventral intermediate portion of the entorhinal cortex

is labeled by virus targeted to the cricothyroid (Figure 12a). This bilateral pattern of infection appears at 96 h. Near the bregma, we observe colabeling in M1 motor cortex, corresponding to a region previously described as the mouse “laryngeal motor cortex” (Arriaga, 2012). This infection is strictly contralateral and emerges at 96 hpi (Figure 12b).

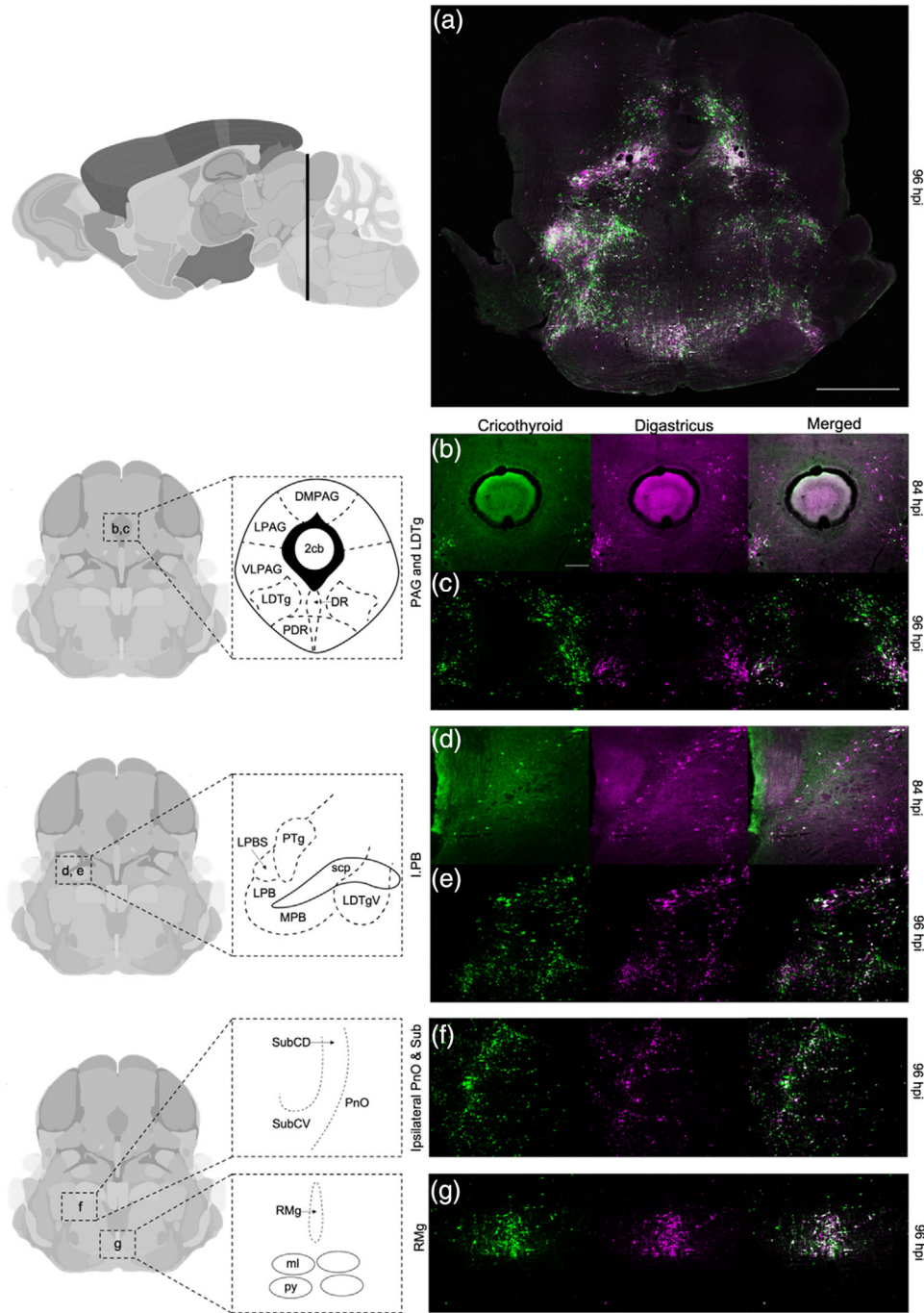


FIGURE 5 Midbrain 1. (a) Tile scan of the midbrain, scale bar = 1 mm. (b) Periaqueductal gray and lateral tegmentum at 84 h postinjection (hpi), scale bar = 200 μ m. (c) Periaqueductal gray and lateral tegmentum at 96 hpi. (d) Ipsilateral parabrachial nucleus at 84 hpi. (e) Ipsilateral parabrachial nucleus at 96 hpi. (f) Pontine reticular nucleus and subcoeruleus at 96 hpi. (g) Raphe magnus at 96 hpi. 2Cb, lobule 2 of the cerebellar vermis; C, contralateral; DMPAG, dorsomedial periaqueductal gray; DR, dorsal raphe; I, ipsilateral; LDTg, laterodorsal tegmental nucleus; LDTgV, laterodorsal tegmental nucleus, ventral part; LPAG, lateral periaqueductal gray; LPBS, lateral parabrachial nucleus, superior part; LPB, lateral parabrachial nucleus; ml, medial lemniscus; MPB, medial parabrachial nucleus; PDR, posterodorsal raphe nucleus; PnO, pontine reticular nucleus, oral part; PTg, pedunculotegmental nucleus; py, pyramidal tract; RMg, raphe magnus nucleus; scp, superior cerebellar peduncle; SubCD, subcoeruleus nucleus, dorsal part; SubCV, subcoeruleus nucleus, ventral part; VLPAG, ventrolateral periaqueductal gray

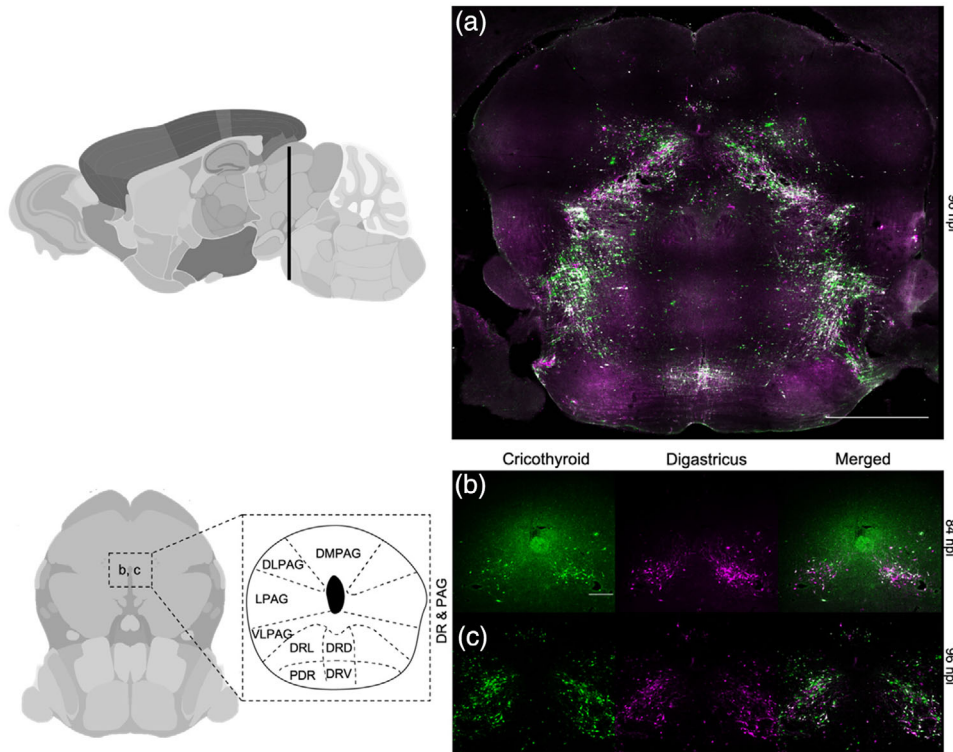


FIGURE 6 Midbrain 2. (a) Tile scan of the midbrain, scale bar = 1 mm. (b) Periaqueductal gray and dorsal raphe at 84 h postinjection (hpi), scale bar = 200 μ m. (c) Periaqueductal gray and dorsal raphe at 96 hpi. DMPAG, dorsomedial periaqueductal gray; LPAG, lateral periaqueductal gray; VLPAG, ventrolateral periaqueductal gray; DLPAG, dorsolateral periaqueductal gray; LPAG, lateral periaqueductal gray; VLPAG, ventrolateral periaqueductal gray; DLPAG, dorsolateral periaqueductal gray; DRD, dorsal raphe nucleus, dorsal part; DRL, dorsal raphe nucleus, lateral part; DRV, dorsal raphe nucleus, ventral part; PDR, posterodorsal raphe nucleus

Lastly, we find a region in the caudal prelimbic cortex (PrL) that is colabeled by the two viruses. At 84 h, this area is sparsely infected by the digastricus virus (Figure 12c), and at 96 h, the overall infection is still sparse, but neurons are doubly labeled with both viruses (Figure 12d).

3.5 | Quantification of singly and doubly labeled neurons

To describe the extent of labeling for each virus, as well as the relative fraction of neurons that are colabeled, we chose a subset of regions that spanned from spinal cord to limbic cortex (Table 3). We report both the average number of cells counted (Table 4) and the percentage colabeled cells projecting to one structure or the other (Figure 13). One structure we report counts from in Table 4 is excluded from our description of percentage of colabeled cells (PrL) due to the low number of infected neurons evident at 96 hpi (Table 4).

We find for regions containing motor neurons (nucleus ambiguus) or muscle-specific sensory neurons (DMPSP5), staining is overwhelmingly ipsilateral and, even at 96 hpi, few neurons are double labeled. The NTS, LPB, and the DMPAG are bilaterally infected by PRV targeted to both muscles, but have very low rates of coinfection (<20%). In contrast, the Gi, LC, MPB, and LPAG had high levels of double-labeled neurons (>40%). All measured forebrain structures had comparably high

levels of coinfection, including the uniquely contralateral infection of the M1 cortex, as well as the bilateral infection of BNST, LH, and PVN. Overall, the pattern of double labeling seemed to be bimodally distributed with a subset of structures exhibiting strong but segregated staining, and others exhibiting high levels of double labeling.

Among brain regions with bilateral expression, we found that rates of double labeling were similar across structures, but the absolute numbers of neurons infected and coinfecting were larger in the hemisphere ipsilateral to the targeted muscles (Table 4; Figure 13).

4 | DISCUSSION

We used two isogenic PRVs to characterize the neural circuits that terminate in muscles of the jaw and larynx, essential effectors of vocalization in the singing mouse, *S. teguina*. This dual-virus approach allows us to identify circuits specific to each of these muscles, as well as identify individual neurons that are upstream of both muscles (Figure 1). From these data, we examine the extent of single- and double-labeled neurons throughout the brain. Lastly, we examine the time of arrival of these vectors (Figure 14). We compare these results to reports from other species to assess whether the pattern of connectivity is consistent with vocal circuits in other vertebrates. Although we report a variety of novel findings, overall our anatomical data are consistent with

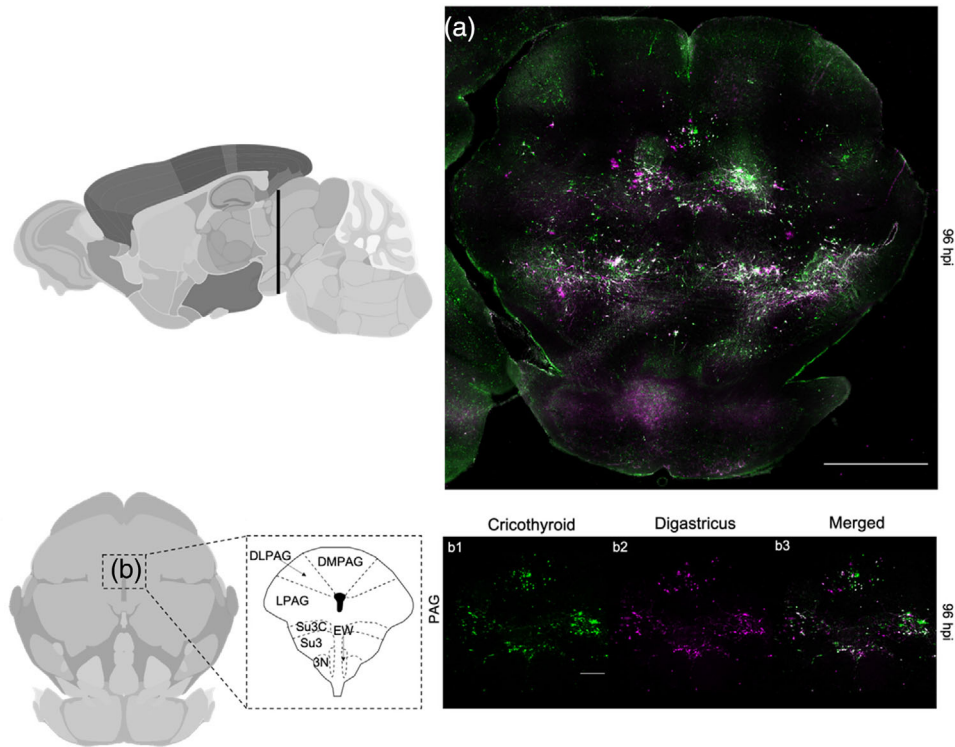


FIGURE 7 Midbrain 2. (a) Tile scan of the midbrain, scale bar = 1 mm. (b) Periaqueductal gray at 96 h postinjection (hpi), scale bar = 200 μ m. 3N, oculomotor nucleus; DMPAG, dorsomedial periaqueductal gray; DLPAG, dorsolateral periaqueductal gray; EW, Edinger-Westphal nucleus; LPAG, lateral periaqueductal gray; SU3, supraoculomotor periaqueductal gray; SU3C, supraoculomotor cap

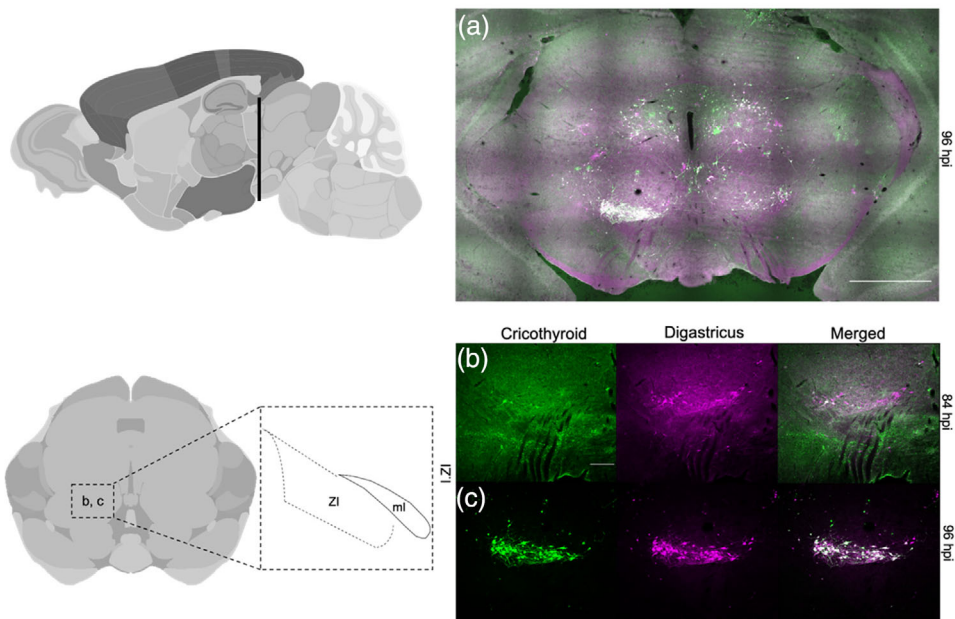


FIGURE 8 Thalamus 1. (a) Tile scan of the thalamus, scale bar = 1 mm. (b) Zona incerta at 84 h postinjection (hpi). (c) Scale bar = 200 μ m, zona incerta at 96 hpi. l, ipsilateral; ml, medial lemniscus; ZI, Zona incerta

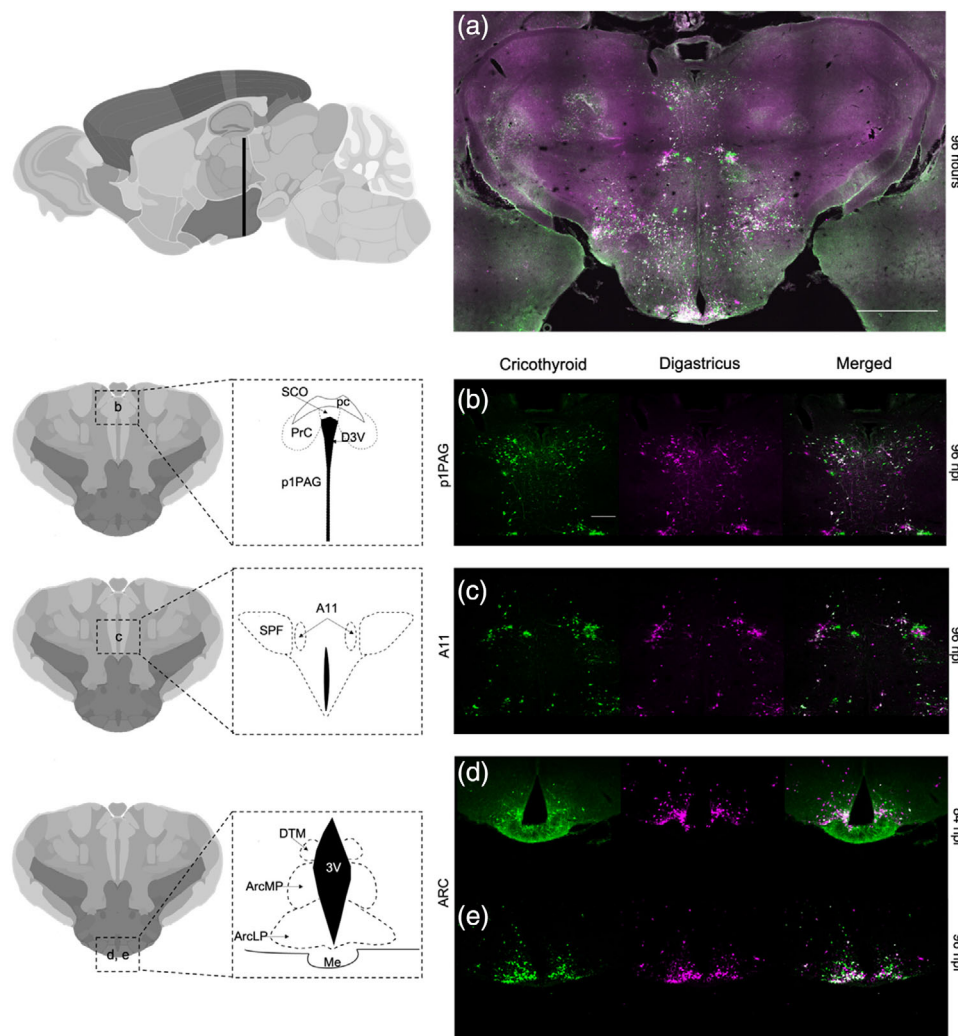


FIGURE 9 Thalamus 2. (a) Tile scan of the thalamus, scale bar = 1 mm. (b) p1 periaqueductal gray at 96 h postinjection (hpi), scale bar = 200 μm . (c) A11 cell population at 96 hpi. (d) Arcuate nucleus at 84 hpi. 93, arcuate nucleus at 96 hpi; 3V, 3rd ventricle; A11, A11 dopamine cells; ArcLP, arcuate hypothalamic nucleus, lateral posterior part; ArcMP, arcuate hypothalamic nucleus, medial posterior part; D3V, dorsal 3rd ventricle; DTM, dorsomedial hypothalamic nucleus; Me, median eminence. p1PAG, p1 periaqueductal gray; pc, posterior commissure; PrC, precommissural nucleus, subcommissural organ

characterizations of forebrain structures implicated in vocalization in other mammals, and with limbic, midbrain, and brainstem compartment patterns described in vocal vertebrates more generally. We now discuss these findings in detail for related regions of interest.

4.1 | Motor neurons and other singly labeled nuclei

The first detection of PRV in the CNS occurs as single-labeled cells in spinal cord compartments that correspond to motor neurons innervating either the larynx (cricothyroid) or the jaw (digastricus). The nucleus ambiguus (NA) is known to contain motor neurons innervating the intrinsic muscles of the larynx, including the cricothyroid. In our study, as in others, the NA is the first to be infected with virus injected into the cricothyroid and contains single-labeled neurons (Figure 2a,b; Arriaga, 2012; Barrett et al., 1994; Cassell, 2010; Hisa, 2016; Waldbaum et al.,

2001). Previous mapping studies suggest that the NA contains distinct fields of neurons specific to particular muscles in the throat. The cricothyroid compartment of the NA occupies a rostral portion of the nucleus, while the other intrinsic laryngeal muscles are more caudal (Hisa et al., 1984). Consistent with this observation, our cricothyroid infection appears rostrally, at the same rostral-caudal level as the inferior olive (Figure 2) (Barrett et al., 1994; Hisa, 2016).

Fewer studies have targeted the anterior digastric muscle (Mercer Lindsay et al., 2019), though for singing mice (and presumably many other species), it is an important vocal muscle (Okobi et al., 2019). The motor neurons innervating the anterior digastricus form a distinct subnucleus (5ADi) that is a ventromedial compartment of the motor trigeminal nucleus (5N) (Franklin & Paxinos, 2007). In our data, we note an early, single-label ipsilateral infection of 5ADi that persists for 96 h (Figure 4a,b). We also find that the ipsilateral motor nucleus of the trigeminal (5N) is sparsely infected (Figure 4c). This is consistent

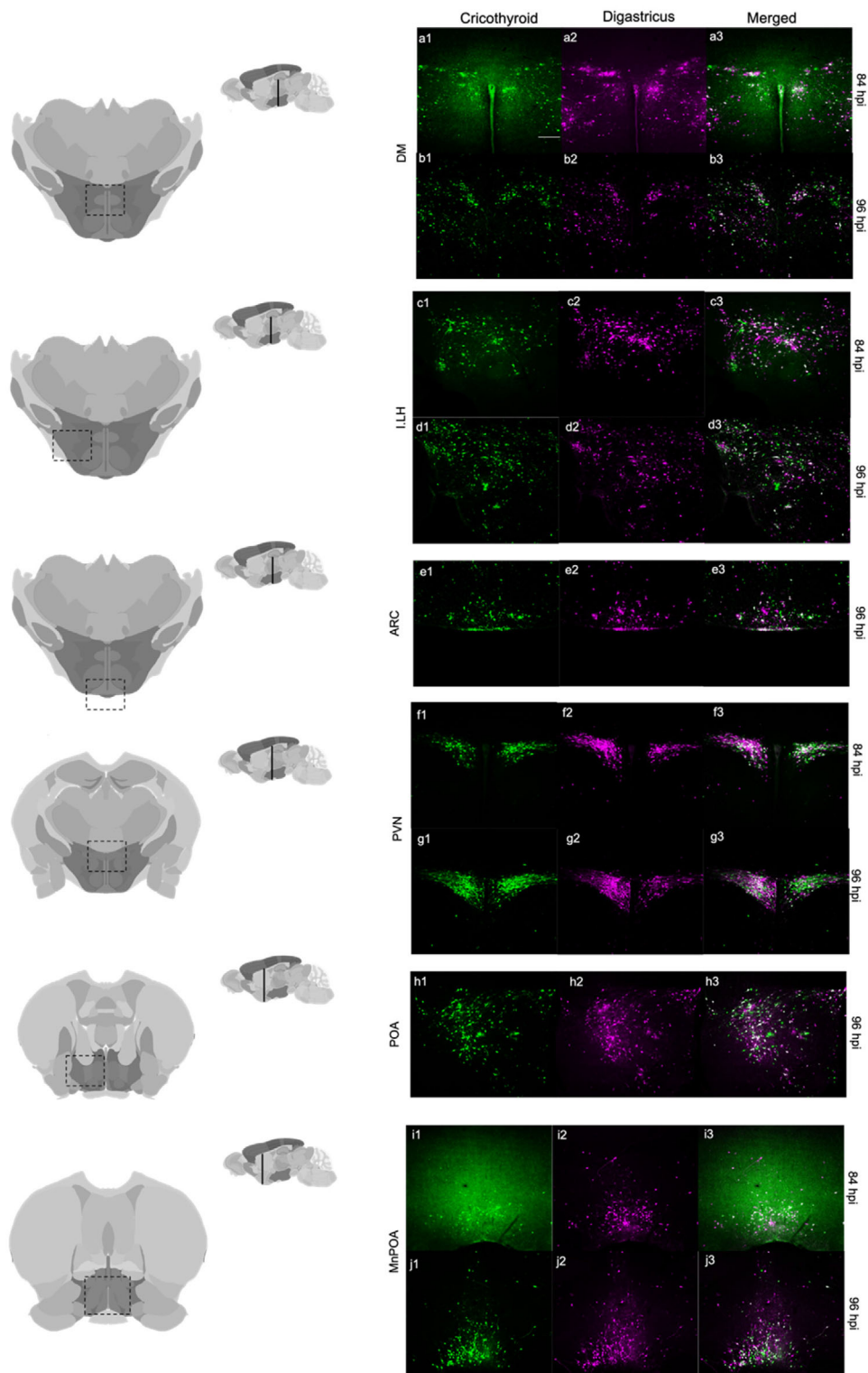


FIGURE 10 Hypothalamus. (a) Dorsomedial hypothalamus at 84 h postinjection (hpi), scale bar = 200 μ m. (b) Dorsomedial hypothalamus at 96 hpi. (c) Ipsilateral lateral hypothalamus at 84 hpi. (d) Ipsilateral lateral hypothalamus at 96 hpi. (e) Arcuate nucleus at 96 hpi. (f) Paraventricular nucleus at 84 hpi. (g) Paraventricular nucleus at 96 hpi. (h) Ipsilateral medial preoptic area at 96 hpi. (i) Median preoptic area at 84 hpi. (j) Median preoptic area at 96 hpi. ARC, arcuate hypothalamic nucleus; DM, dorsomedial hypothalamic nucleus; I, ipsilateral; LH, lateral hypothalamus; MnPOA, median preoptic nucleus; POA, preoptic area; PVN, paraventricular hypothalamic nucleus

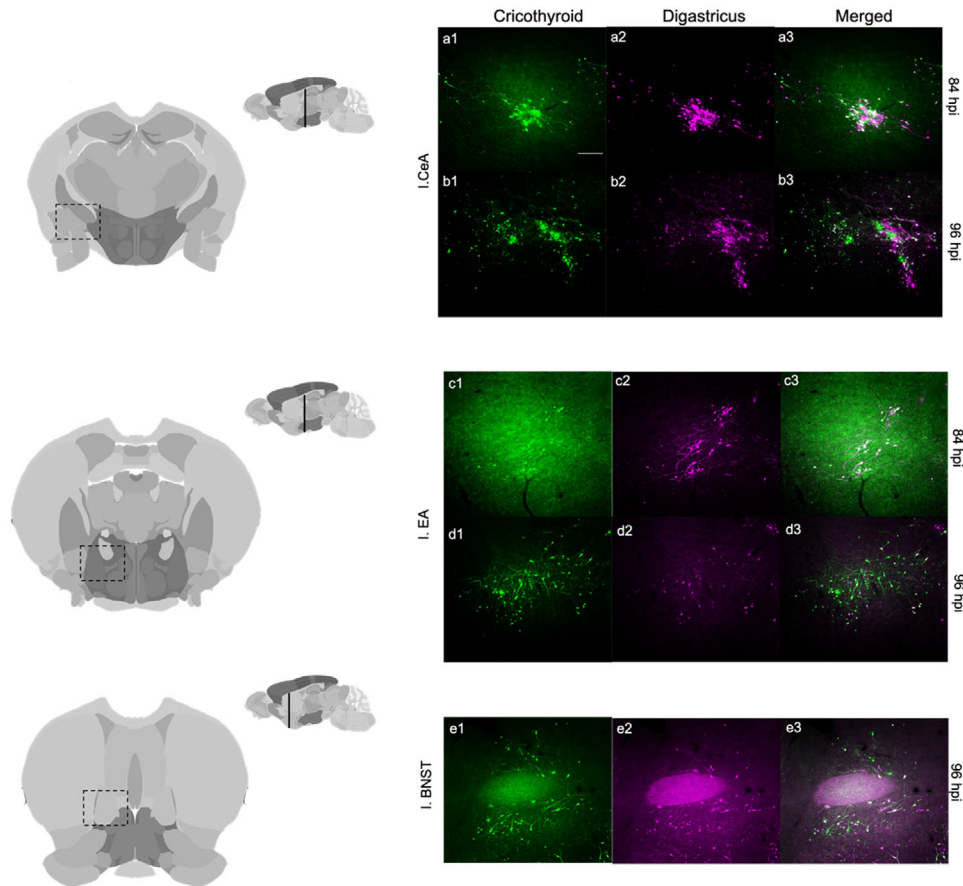


FIGURE 11 Amygdala. (a) Central amygdala at 84 h postinjection (hpi), scale bar = 200 μ m. (b) Central amygdala at 96 hpi. (c) Extended amygdala at 84 hpi. (d) Extended amygdala at 96 hpi. (e) Ipsilateral bed nucleus of the stria terminalis at 96 hpi. BNST, bed nucleus of the stria terminalis; CeA, central amygdala; EA, extended amygdala; I, ipsilateral

with horseradish peroxidase (HRP) and PRV studies targeting the anterior digastric belly of the muscle of rats (Kang et al., 1999; Kemplay & Cavanagh, 1983).

In addition to motor neurons of the jaw and larynx, we also found a predominant ipsilateral single label of the spinal trigeminal nucleus oralis (DMSP5) (Figures 2d and 13; Table 4). This nucleus is considered a somatosensory nucleus and also has been labeled in monosynaptic retrograde studies of the masseter and digastric (Iv et al., 2014; Mercer Lindsay et al., 2019). Given the importance of the anterior digastric muscle in the vocalizations of *S. teguina* (Okobi et al., 2019) specifically with gape and frequency modulation, we speculate that this nucleus may provide sensory feedback on jaw movement during vocalization and other activities.

We find bilateral infection of the nucleus of the solitary tract (NTS) (Figure 2d,e), a pattern observed in previous work (Arriaga et al., 2015; Barrett et al., 1994; Hisa, 2016). The NTS is often considered upstream of motorneuron pools, as a primary premotor nucleus and as a second-order regulator of the nucleus ambiguus. We find that this structure and many of its sub-compartments are infected by PRV originating in the cricothyroid. A subset of neurons are labeled with PRV originating in the digastricus, but relatively few neurons are double labeled (Table 4; Figure 13). This suggests that the structure is heterogeneous in

function; although it seems positioned to influence both muscle groups, few cells seem equipped to coordinate both muscles. Its strong expression in the ipsilateral side by the digastric infection suggests independent modulation of jaw function. Functional tests of this region have implicated it in innate vocalization and tied it to the expiratory phase of breathing (Hernandez-Miranda et al., 2017).

4.2 | Putative central pattern generators

The *Scotinomys* song is a rhythmic and frequency-modulated trill that involves the coordination of larynx, jaw, and respiratory muscles to produce each note (Campbell et al., 2010; Okobi et al., 2019; Pasch et al., 2011b). The notes themselves are repeated and stereotyped, and acoustic changes over the course of the song are well-described by a polynomial function (Campbell et al., 2010). This highly rhythmic and repeated coordination of movements suggests the activity of one or more central pattern generators; we would expect such CPGs to be double labeled bilaterally, to reside within the brainstem or spinal cord, and to be among the first structures doubly labeled.

Work on vocalization and orofacial pattern generation generally suggests that CPGs for vocal behavior would be located in the

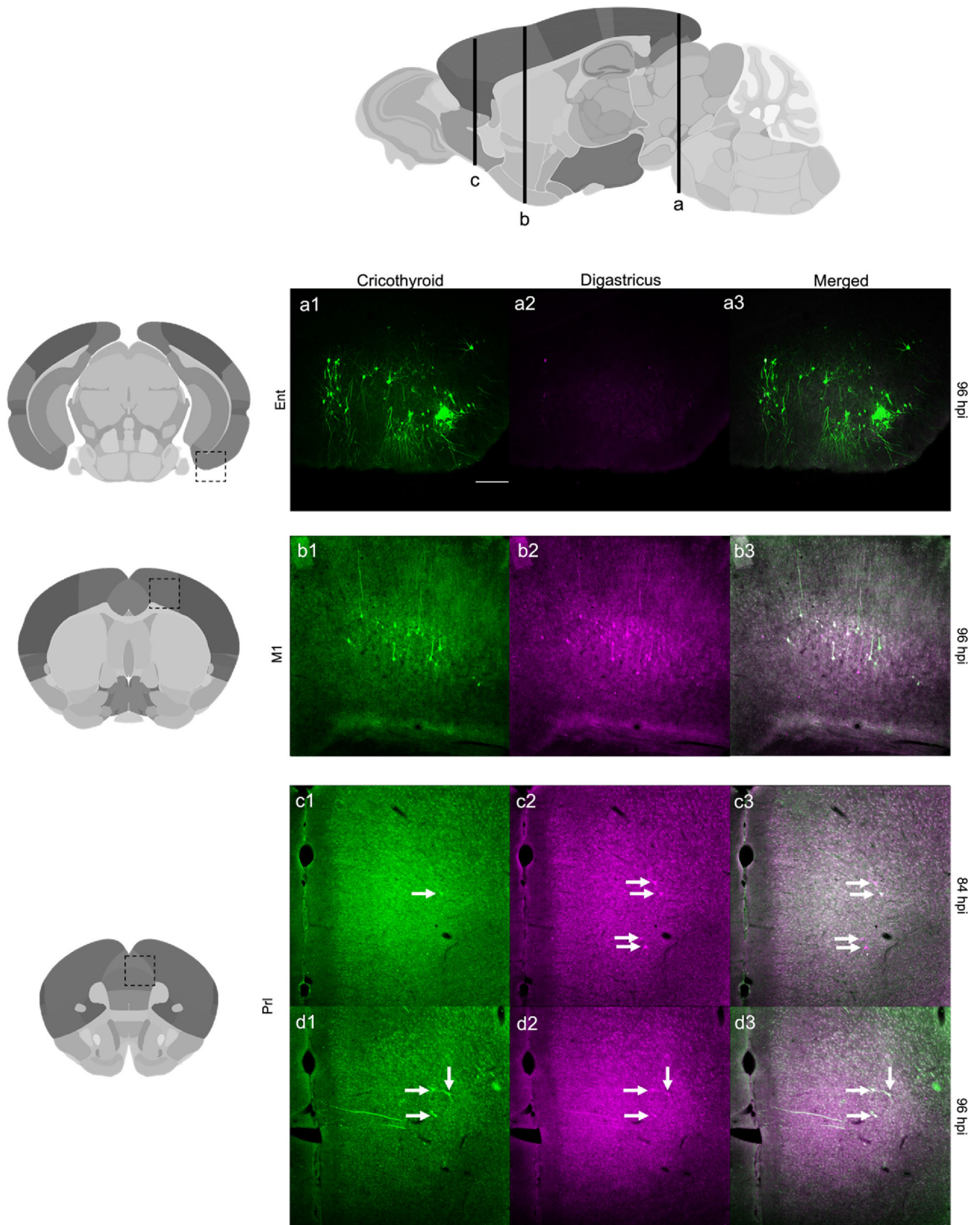


FIGURE 12 Cortex. (a) Contralateral entorhinal cortex at 96 h postinjection (hpi), scale bar = 200 μ m. (b) Primary motor cortex at 96 hpi. (c) Prelimbic cortex at 84 hpi and 96 hpi. Ent, entorhinal cortex; M1, primary motor cortex; PrL, prelimbic cortex; Arrows denote cell bodies on the PrL

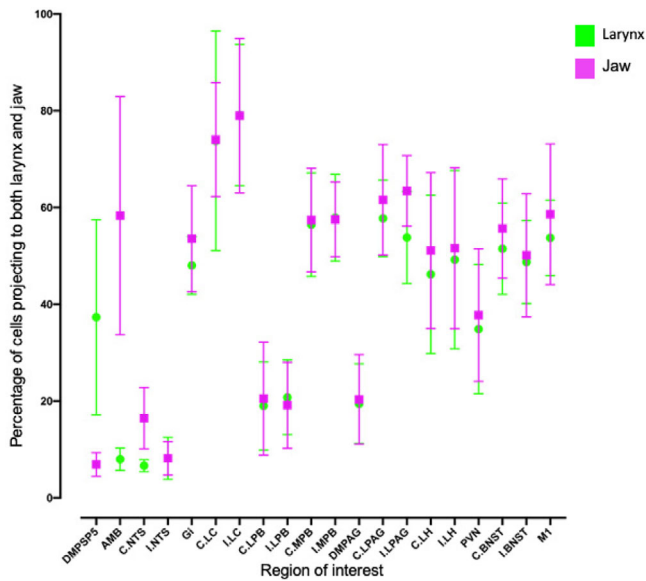


FIGURE 13 Quantification and variation in colabeled cells projecting to cricothyroid (larynx) and anterior digastricus (jaw) across regions of interest analyzed at 96 h postinjection (hpi) ($n = 5$). Error bars = standard deviation. AMB, nucleus ambiguus; BNST, bed nucleus of the stria terminalis; C., contralateral; DMPSP5, dorsalmedial trigeminal nucleus; DMPAG, dorsomedial periaqueductal gray; Gi, gigantocellular reticular nucleus; I., ipsilateral; LC, locus coeruleus; LH, lateral hypothalamus; LPAG, lateral periaqueductal gray; LPB, lateral parabrachial nucleus; M1, primary motor cortex; MPB, medial parabrachial nucleus; NTS, nucleus of the solitary tract; PVN, paraventricular nucleus; ROI, region of interest

brainstem (Barlow, 2009; Bass, 2014; Bass & Ramage-healey, 2008; Hage, 2010; Moore et al., 2014; Rhodes et al., 2007). Among the many CPGs implicated in orofacial movements (Moore et al., 2014), Hage (2010) suggests five candidates for patterning of vocal behavior specifically. These include the parvocellular reticular nucleus (PCRT), pontine reticular nucleus (PnO), the nucleus retroambiguus (NRA), the nucleus raphe magnus (RMg), and the lateral paragigantocellular reticular (LPGi) formation.

Among these regions, the LPGi labeling is most consistent with our expectations of a CPG. It is labeled at the earliest timepoint (72 hpi), largely double labeled, and bilaterally infected (Figures 2a, 3a, and 13; Table 4). The pattern of double-labeled neurons forms a large medial structure that not only spans the LPGi but also extends throughout the gigantocellular reticular formation (Gi) and raphe obscurus (ROb)—structures that have been identified as orofacial pattern generators, but were not identified as putative vocal pattern generators (Hage, 2010; Moore et al., 2016).

Among three other putative CPGs, we find labeling that seems inconsistent with expectations for a vocal pattern generator. For example, expression of the digastricus and cricothyroid labels in the PCRT is largely segregated by muscle (Figure 3d,e). Both the PnO and RMg exhibit double labeling, but the viruses do not arrive in either structure until 84 hpi, a time point that coincides with expression in the hypothalamus and other upstream structures (Figure 5f,g). Lastly, the

NRA is at the caudal boundary of our tissue sampling, so we did not reliably obtain sections for examination; the literature supporting its role in vocalization (Tschida et al., 2019) suggests that it would be worth examining this structure in a more targeted way.

From our current data, the LPGi, contiguous Gi and ROb would seem to be the strongest candidates for CPGs governing song production. However, there are a variety of models that describe how CPGs may control orofacial movements including vocalizations (Hage, 2010; Stanek IV et al., 2014), and it is possible that one or more of additional brainstem regions may influence patterning of the *Scotinomys* song.

4.3 | Neuromodulatory regions

We find several regions within the pons that are known to express either neuropeptides or catecholamines and exhibit robust double labeling at 84 hpi. We interpret these structures as neuromodulatory regions.

Our study points to a strong role of catecholamines in the modulation of vocal behavior in this species. The noradrenergic A5 and A6 (locus coeruleus, LC) populations are coinfecting by the two PRV strains (Figure 3b–e). Indeed, LC exhibits an even higher degree of colocalization than the Gi (Figure 13; Table 4). The LC is the major center for norepinephrine synthesis in the brain (Samuels & Szabadi, 2008). It has major connections throughout the neuraxis (Szabadi, 2013) including the nucleus ambiguus, dorsal motor root of the vagus, and the gigantocellular reticular formation. The LC has been indirectly implicated in ultrasonic vocalizations (Hamed & Boguszewski, 2018) and is more broadly involved in wakefulness, arousal, and sensory processing (Aston-Jones & Cohen, 2005; Samuels & Szabadi, 2008). Interestingly, the LC influences perception of rodent vocalizations through its projections to the auditory cortex (Foote et al., 1975; Martins & Froemke, 2015; Sara, 2009). Perhaps more closely related to the current study, the cell groups of A5 and A6 also play antagonistic roles in the regulation of respiratory rhythms (Guyenet et al., 1993; Hilaire et al., 2004). The neural circuitry underlying breathing is obviously of broad relevance to vocalization in general (Barkan & Zornik, 2020), and in singing mice, each note of its song is accompanied by a short breath (Okobi, 2016; Pasch et al., 2011a).

We also observe coinfection in the dopaminergic A11 population of cells (Figure 9c). Like the noradrenergic populations, these neurons are known to have roles in auditory processing (Nevue et al., 2016) as well as motor functions (Koblinger et al., 2014). Interestingly, our dopaminergic results contrast with work that emphasizes the role of dopamine in other taxa (Saravanan et al., 2019; Simonyan et al., 2012), in that our TH/PRV triple-labeling revealed no PRV infection in either the ventral tegmental area or the substantia nigra pars compacta (Figure 15b).

The parabrachial nucleus (PBN) expresses a variety of neuropeptides and is known for its role in vocal–respiratory interactions (Smotherman et al., 2010). The structure is topographically organized in terms of lateral, ventrolateral, and medial regions surrounding the superior cerebellar peduncle (Franklin & Paxinos, 2007). In our study, the medial division has the highest abundance of double-labeled cells (Figure 13;

Table 4). This division has reciprocal connections with the nucleus ambiguus (Herbert et al., 1990; Núñez-Abades et al., 1990; Saper & Loewy, 1980) and receives inputs from much of the forebrain, including limbic regions that are canonical parts of the mammalian vocal circuit, such as hypothalamus, amygdala, anterior cingulate cortex (ACC), and laryngeal motor cortex (LMC; Jürgens, 2002). Recordings in cats show that the medial PBN fires along with vocal and respiration behaviors (Farley et al., 1992). In free-tailed bats (*Tadarida brasiliensis*), *c-fos* immunoreactivity is detected in the medial (and lateral) parabrachial nucleus after calling (Schwartz & Smotherman, 2011). It is hypothesized that the medial subdivision of the parabrachial nucleus modulates laryngeal activity for the purpose of vocalizations, while the lateral is directed toward vocal–respiratory coupling (Smotherman et al., 2010). The extensive double labeling apparent in our experiment suggests that the parabrachial nucleus may more broadly coordinate vocal muscles (Figures 4g and 5e).

4.4 | The midbrain

The periaqueductal gray (PAG) is considered one of the most crucial centers for mammalian vocalization (Gruber-Dujardin, 2010; Jürgens, 2002). Multiple lines of evidence point to this large heterogeneous structure as one for “gating” of downstream vocal output (Esposito et al., 1999; Jürgens, 1994; Tschida et al., 2019). Anatomically, it stretches rostrally to the hypothalamus and caudally to the pontine nucleus of the brainstem (Gruber-Dujardin, 2010). The structure has been subdivided by Bandler and Keay (1996) along its longitudinal axis into four columns: the dorsomedial PAG (dmPAG), dorsolateral PAG (dlPAG), lateral PAG (LPAG), and ventrolateral PAG (VLPAG) (Bandler & Keay, 1996; Kingsbury et al., 2011). These subdivisions are thought to serve different functional domains and promote different types of vocal output (Dujardin & Jürgens, 2006). Our data highlight distinctions among these subdivisions (Figures 5–9).

Among PAG compartments, the VLPAG is the first to exhibit coinfection (84 hpi) and is labeled throughout its rostro-caudal axis. Among the remaining compartments, the LPAG has the higher coinfection (Figure 13). The DMPAG has robust infection by both viruses, but few doubly labeled cells (Table 4). Moreover, label in the DMPAG does not arrive until 96 hpi. Together, the data suggest that the LPAG and VLPAG are more likely to regulate vocalization in *S. teguina*. This heterogeneity among PAG regions is consistent with tracing studies targeting the jaw and/or larynx of laboratory rodents (Bennett et al., 2019; Falkner et al., 2020; Fay & Norgren, 1997; Tschida et al., 2019). Moreover, among both mammals and birds, the LPAG is thought to be particularly important for vocalizations (Dujardin & Jürgens, 2006; Kingsbury et al., 2011).

4.5 | The hypothalamus

The hypothalamus is a major modulator of vocal behavior (Adkins-Regan, 2005; Hage, 2010; Hage & Nieder, 2016; Nieder & Mooney,

2020). In singing mice, hypothalamic areas such as POA, PVN, and LH all show medium to high levels of coinfection by the two strains of the virus (Figure 13; Table 4). The POA and the PVN are intricately involved in courtship and aggressive behaviors (Wei et al., 2018) and are canonical regions of a social behavior network important across vertebrates (O’Connell & Hofmann, 2011; Goodson, 2005; Newman, 1999). We find dense colabeling in both the medial preoptic area and the median preoptic area (Figure 10h–j). The MPOA is implicated vocal and courtship behavior across vertebrates (Goodson & Bass, 2000; Schmidt, 1968), and in the generation of rodent ultrasonic vocalizations specifically (Gao et al., 2019; Michael et al., 2020). Studies of squirrel monkeys implicate the dorsomedial hypothalamus (DM) in species-specific calls (Jürgens, 1982; Jürgens & Ploog, 1970), most likely due to its connections with the PAG (Dujardin & Jürgens, 2006); we find doubly labeled cells in the DM, but they are restricted to a subset of the nucleus (Figure 10a,b).

The ARC, PVN, and LH (Figures 9d,e and 10c–g) are interconnected nuclei that regulate energy balance in part through effects on feeding and other behaviors (Larsen et al., 1994; G. J. Morton et al., 2006; Stuber & Wise, 2016). One of the many studies implicating these regions in energy balance is a double-PRV study showing viruses injected into liver and adipose tissue converge on neurons within these hypothalamic structures (Stanley et al., 2010). The confluence of social and feeding circuits within the PVN in particular suggests that it is well-positioned to play a role in the modulation of vocal effort by energy balance, a pattern known in singing mice, as well as many other species (Burkhard et al., 2018; Giglio & Phelps, 2020; E. S. Morton, 2017).

4.6 | The extended amygdala

The amygdala complex plays a central role in a diversity of motivated behaviors, many of which are social (Newman, 1999). The lateral septum (LS), central amygdala (CeA), and bed nucleus of the stria terminalis (BNST) have all been implicated in vocalization across diverse taxa (see below). In *Scotinomys*, we find colabeling from larynx and jaw in the CeA, BNST, and in the extended amygdala (*sensu* Franklin & Paxinos, 2007). The EA and CeA both are coinfecting at 84 h (Figure 10a–d), while we did not detect double labeling in the BNST and LS until 96 h (Figure 10e). Even at 96 h, LS labeling was relatively sparse, suggesting it is upstream of amygdala or hypothalamic structures. In lab mice, the EA and CeA inhibit the production of USVs through descending projections to the PAG (Michael et al., 2020). In contrast, electrical stimulation of the amygdala can elicit vocalizations in a variety of mammals, including the mustache bat (Ma & Kanwal, 2014), guinea pig (Green et al., 2018), domestic pig (Manteuffel et al., 2007), and squirrel monkey (Jürgens et al., 1967). Similarly, stimulation of the BNST elicits calls in the rhesus macaque (Robinson, 1967) and squirrel monkey (Jürgens & Ploog, 1970). In *Xenopus* frogs, stimulation of the CeA and BNST evokes fictive calling (Hall et al., 2013).

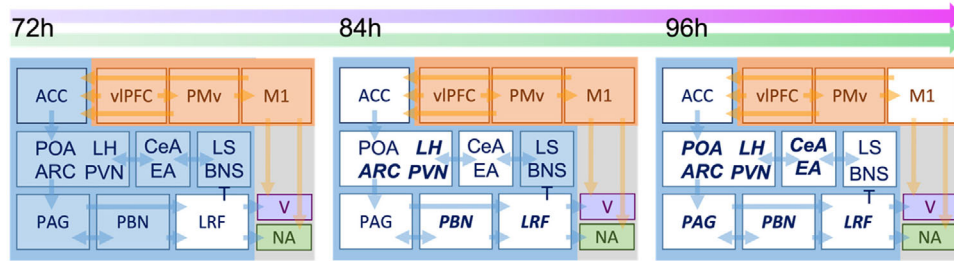


FIGURE 14 Summary. Time course description of current PRV study. Blue represents the nodes of the primary vocal motor network as defined by Hage and Nieder (2016). Orange presents the nodes of the volitional articulatory motor network. Green and purple represent the infection by one of the strains of the virus. White represents evidence of colabeling of both viruses. Bold letters represent extensive infection of PRV in nuclei. V, motor trigeminal nucleus and motor trigeminal nucleus, anterior digastric portion; ACC, anterior cingulate cortex as putatively defined by Bennet et al. (2019) to be a subcompartment of the prelimbic cortex. ARC, arcuate nucleus; BNST, bed nucleus of the stria terminalis; CeA, central amygdala; EA, extended amygdala; LH, lateral hypothalamus; LRF, lateral reticular formation; LS, lateral septum; M1, primary motor cortex; NA, nucleus ambiguus; PAG, periaqueductal gray; PBN, parabrachial nucleus; PMv, ventral premotor cortex; POA, preoptic area; viPFC, ventrolateral prefrontal cortex. Note: arrows do not represent monosynaptic relationships

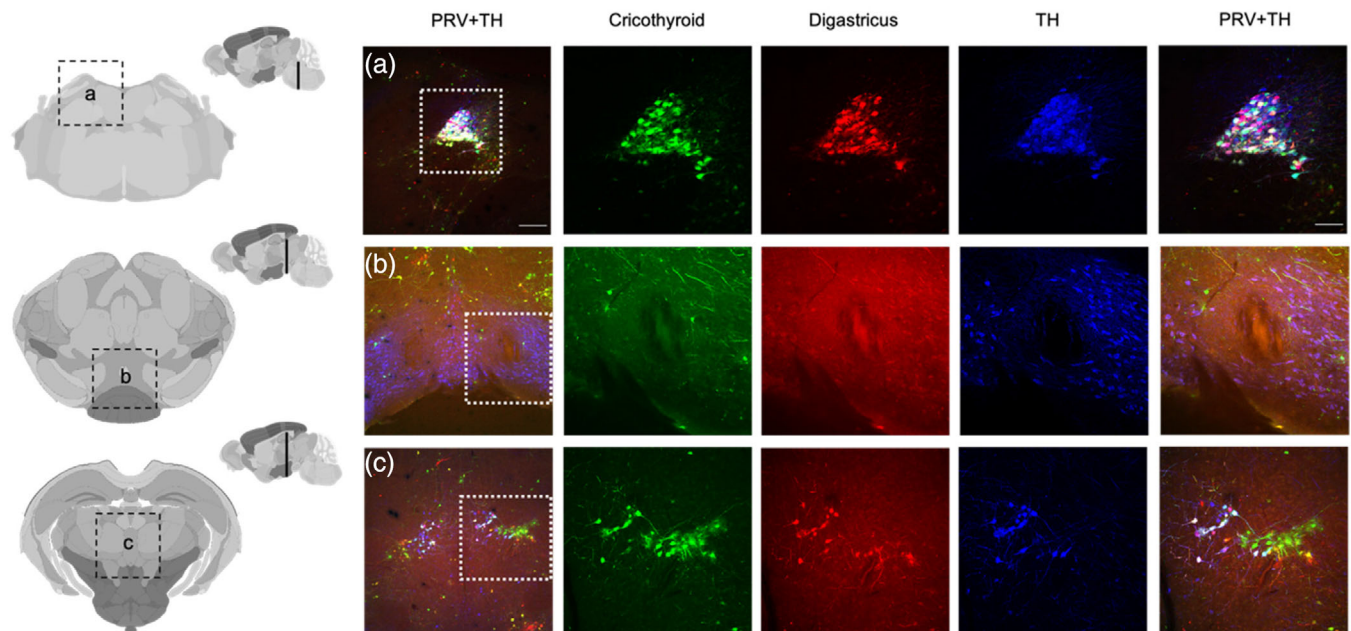


FIGURE 15 Tyrosine hydroxylase triple labeled structures. (a) Locus coeruleus triple labeled, scale bar = 200 μm , PRV + TH scale bar = 100 μm . (b) Ventral tegmental area triple labeled. (c) A11 and subparafiscal nucleus triple-labeled. PRV, pseudorabies virus; TH, tyrosine hydroxylase

4.7 | The cortex

We found three distinct cortical regions that were labeled with PRV—M1 motor cortex, prelimbic cortex (PrL), and entorhinal cortex (Ent) (Figure 12a–c). The LMC, a region of M1 near the bregma, was infected only on the side contralateral to the injection, a finding consistent with studies of lab mice (Arriaga et al., 2012; Chabout et al., 2016; Komiyama et al., 2010). The rodent LMC is thought to be homologous to human LMC, which is essential for speech (Simonyan, 2014). To our knowledge, our study is the first to examine whether the M1 neurons that connect to laryngeal muscles are also connected to other muscles important for vocalization. Because most M1 neurons were double labeled, the region might better be regarded as a vocal motor

cortex, rather than laryngeal cortex per se. The rodent prelimbic cortex (PrL) has also recently been implicated in vocalization. Working in rats, Bennett et al. (2019) argue that the posterior prelimbic cortex is connected to the LPAG, and that it may be homologous to the monkey ACC, which has long been recognized as an important area for vocal output in primates (Jürgens, 2009). In *S. tiguina*, we find that specific regions within the PrL show bilateral, coinfecting neurons. This labeling, however, shows up sparsely at 96 hpi, the final time point sampled. Lastly, a region of the entorhinal cortex (Ent) is infected bilaterally. Unlike the other regions, however, its label derives predominantly from the larynx. Although not canonically a “vocal” structure, it has been previously reported as being positively infected by a larynx-infected PRV circuit in the brain of rats (Van Daele & Cassell, 2009).

4.8 | Uses and limitations of PRV

The primary advantage of our dual-PRV approach is the rapid, circuit-level delineation of brain regions and neurons that modulate one or both muscles (Callaway, 2008; Hogue et al., 2018; Saleeba et al., 2019). We can also ask whether the timing of infection is consistent with networks identified in other species. Before discussing such interpretations, it is worthwhile to provide some caveats. The first is that in dual-labeling studies with virally infected neurons, the presence of one virus infection might limit infection by a second, a phenomenon known as the “principle of exclusion” or “superinfection inhibition” (Doslikova et al., 2019; Kobiler et al., 2010; Saleeba et al., 2019). The widespread and region-specific presence of double labeling in our study, however, suggests that this may not be a major concern (Figure 13). A second caveat is that there is evidence that the virus may sometimes infect fibers of passage (S. Chen et al., 1999). However, this finding stemmed from local injection of PRV into a brain region. In our study, targeting of muscles makes this form of infection unlikely. A third caveat is that PRV is large viral particle and is thought to be heavily biased toward synapses that are on or near the soma. This would not invalidate our infected regions but would suggest that they are a subset of the total vocal circuit. Fourth, the time of arrival of the virus provides only a rough estimate of connectivity. While this approach is thus poorly suited for definitively characterizing projections, it is an excellent way to quickly delineate a circuit in a novel species and compare results to existing networks. Finally, PRV has been shown to cause neuronal degeneration in infected neurons (Ugolini, 2010); this may cause loss of labeling in early-infected structures observed at later time points. For example, in Figure 2b, dense digastricus labeling in the pre-BotC is evident at 72 h, but disappears by 96 h.

Although we targeted the cricothyroid and digastricus muscles, our results are remarkable concordant with a detailed single-label anatomical study that injected PRV into another intrinsic laryngeal muscle, the thyroarytenoid (Van Daele & Cassell, 2009). Although the study was done in rats, both the identified brain regions and their times of arrival were quite similar to those we report. One notable difference is that these authors report ipsilateral infection for several forebrain structures—we found no strictly ipsilateral connections above the level of the brainstem, though most *Scotinomys* forebrain structures labeled more strongly ipsilaterally than contralaterally. Both studies, however, show some bilateral infection of most forebrain structures, so the overall pattern is one that is bilateral but biased toward ipsilateral infection. The uniquely contralateral infection in M1 cortex in singing mice and lab rats is one exception to this overall trend (Van Daele & Cassell, 2009; see also Arriaga et al., 2012 for similar results with lab mice).

5 | CONCLUSIONS

Taken together, our findings outline a vocal motor circuit that spans from motor neurons to limbic cortex. At the level of the hypothalamus, amygdala, midbrain, brainstem, and spinal cord, the regions infected by the virus are remarkably concordant with vocal circuits reported for a variety of vertebrates. The CeA, MPOA, and BNST, for example,

all regulate vocalization in frogs (Bass & Remage-healey, 2008). Similarly, the PAG is a recurring and central player in the regulation of vocalization across vertebrate species (Kittelberger & Bass, 2013). Our identification of cortical structures is consistent with recent reports in laboratory rodents and established circuits of vocalization in primates (Bennett et al., 2019; Jürgens, 2009). Such patterns suggest that these cortical contributions likely date to at least the common ancestor of the clade euarchontoglires – the mammalian group defined to include rodents, tree shrews, bushbabies and primates—though they may prove to be older still. It would be particularly interesting to know how ancient these cortical/pallial circuits are. Outside of songbirds, whose vocal circuits are derived and specialized (Sakata & Yazaki-Sugiyama, 2020), little work has been done to characterize pallial components of vocal circuits in non-mammals. These would clearly be interesting areas for further research. Overall, our data, and the literature as a whole, suggest a general conservation of vocal circuitry across broad taxonomic scales.

Given the elaboration of vocalization in singing mice, and the fact that they are separated from laboratory rodents by roughly 40 million years of evolution (Steppan & Schenk, 2017), we thought that we might see novel aspects of vocal circuitry. In contrast, the architecture of vocalization seems broadly similar to that reported in laboratory rodents. Thus, the elaboration of vocalization does not seem to have been accompanied by gross changes in neural architecture—or at least none discernible with our current methods. We find three possible exceptions. One is the large doubly labeled field within the reticular formation (LPGi, Gi, ROb), which we hypothesize may play an important role in the patterning of *Scotinomys* song. This seems likely to be a novel elaboration of vocal circuitry in the singing mouse. A second is the high level of bilateral infection we see in this circuit compared to some other reports (Doslikova et al., 2019; Hettigoda et al., 2015). The third and final difference is that most models of mammalian vocalization posit that descending forebrain projections from the hypothalamus influence vocalization through effects on the PAG (Jürgens, 2002; Tschida et al., 2019); in our data, however, robust double labeling within PAG appeared either coincident with or following double labeling in the hypothalamus—a pattern that suggests the hypothalamus may have some modulatory role that is not mediated by the PAG. Interestingly, work from Chen et al., 2021, in lab mice has identified a direct projection from the preoptic hypothalamus to the nucleus ambiguus (Chen et al., 2021); stimulation of these neurons, however, did not elicit vocalization, and so their functions remain unknown. Thus, while projections from the hypothalamus to the brainstem are not included in common models of mammalian vocal pathways, data from other rodents suggest that it is likely not unique to *Scotinomys*. Additional work is needed to identify its functions.

In addition to improving our understanding of the evolution and conservation of mammalian and vertebrate vocal circuits, we also hoped to gain insights into the neural mechanisms that might underlie the complex decisions that mediate the adaptive modulation of advertisement displays. Among singing mice, as in many other taxa, display effort is influenced by reproductive state and body condition (Burkhard et al., 2018; Giglio & Phelps, 2020; Pasch et al., 2011b). In another study (Zheng et al., 2021), we identify the presence of

androgen receptors across this broad circuit, providing a potential mechanism for the androgen-dependence of *Scotinomys* song (Pasch et al., 2011). We have also found that body condition in general, and circulating leptin specifically, is associated with individual differences vocal effort. In this context, the extensive double labeling in the PVN is particularly interesting. The structure is at the nexus of limbic regions known as the social behavior network (Newman, 1999), and the hypothalamic circuits of energy balance (G. J. Morton et al., 2006). This structure seems to be a good candidate for the integration of social, reproductive, and energetic information related to display in general, and to vocal behavior in particular.

In summary, this study employed a combination of viruses to target two distinct muscles in the larynx and jaw and identify neurons that were double labeled by both retrograde viral tracers. Although known motor neurons were singly labeled, as expected, we found extensive double labeling at many higher levels. This circuit tracing suggests novel candidates for CPGs driving song, common limbic structures identified in other vertebrate groups, and cortical structures recently implicated in the control of vocalization in laboratory rodents as well as primates. We find that the circuitry seems broadly conserved across species and find no evidence of major circuit rearrangements associated with the elaboration of song in this novel model species. Lastly, our anatomical data suggest candidate brain regions for the integration of interoceptive and exteroceptive cues needed to produce adaptive variation in vocal behavior. We suggest that the dual-label approach, with PRV as well as with other transsynaptic tracers, is an excellent way to quickly characterize vocal circuits in nonmodel mammals. Such studies will be important to our understanding of natural diversity in brain, behavior, and evolution.

ACKNOWLEDGMENTS

We would like to thank Dr. Lynn Enquist for generously providing PRV-152 and PRV-614 through the Center for Neuroanatomy and Neurotropic Viruses (CNNV). We would also like to thank Dr. Gustavo Arriaga for consultation on the cricothyroid injection. Funding for this project was made possible through P40 OD010996 to CNNV, 5R01NS113071 to Michael A. Long and Steven M. Phelps, NSF IOS-1457350 to SMP. We would also like to thank the feedback of two anonymous reviewers which improved the manuscript.

CONFLICT OF INTEREST

The author declares no conflict of interest.

DATA AVAILABILITY STATEMENT

The data that support the findings of this study are available from the corresponding author upon reasonable request.

ORCID

Da-Jiang Zheng  <https://orcid.org/0000-0002-0081-8385>

Daniel E. Okobi Jr  <https://orcid.org/0000-0001-8421-0723>

Samantha K. Smith  <https://orcid.org/0000-0003-4491-1028>

Michael A. Long  <https://orcid.org/0000-0002-9283-3741>

Steven M. Phelps  <https://orcid.org/0000-0002-1095-361X>

REFERENCES

- Adkins-Regan, E. (2005). *Hormones and animal social behavior* (1st ed.). Princeton University Press.
- Arriaga, G. (2012). Of mice, birds, and men: The mouse ultrasonic song system and vocal behavior. *Dissertation Abstracts International, B: Sciences and Engineering*, 72(7), 3859. <https://doi.org/10.1371/journal.pone.0046610>
- Arriaga, G., Macopson, J. J., & Jarvis, E. D. (2015). Transsynaptic tracing from peripheral targets with pseudorabies virus followed by cholera toxin and biotinylated dextran amines double labeling. *Journal of Visualized Experiments*, 103, e50672. <https://doi.org/10.3791/50672>
- Arriaga, G., Zhou, E. P., & Jarvis, E. D. (2012). Of mice, birds, and men: The mouse ultrasonic song system has some features similar to humans and song-learning birds. *PLoS One*, 7(10), e46610. <https://doi.org/10.1371/journal.pone.0046610>
- Aston-Jones, G., & Cohen, J. D. (2005). An integrative theory of locus coeruleus-norepinephrine function: Adaptive gain and optimal performance. *Annual Review of Neuroscience*, 28(1), 403–450. <https://doi.org/10.1146/annurev.neuro.28.061604.135709>
- Bandler, R., & Keay, K. A. (1996). Columnar organization in the mid-brain periaqueductal gray and the integration of emotional expression. *Progress in Brain Research*, 107, 285–300. [https://doi.org/10.1016/S0079-6123\(08\)61871-3](https://doi.org/10.1016/S0079-6123(08)61871-3)
- Banerjee, A., Phelps, S. M., & Long, M. A. (2019). Singing mice. *Current Biology*, 29(6), R190–R191. <https://doi.org/10.1016/j.cub.2018.11.048>
- Banfield, B. W., Kaufman, J. D., Randall, J. A., & Pickard, G. E. (2003). Development of pseudorabies virus strains expressing red fluorescent proteins: New tools for multisynaptic labeling applications. *Journal of Virology*, 77(18), 10106–10112. <https://doi.org/10.1128/jvi.77.18.10106-10112.2003>
- Barkan, C. L., & Zornik, E. (2020). Inspiring song: The role of respiratory circuitry in the evolution of vertebrate vocal behavior. *Developmental Neurobiology*, 80(1–2), 31–41. <https://doi.org/10.1002/dneu.22752>
- Barlow, S. M. (2009). Central pattern generation involved in oral and respiratory control for feeding in the term infant. *Current Opinion in Otolaryngology & Head and Neck Surgery*, 17(3), 187–193. <https://doi.org/10.1097/MOO.0b013e32832b312a>
- Barrett, R. T., Bao, X., Miselis, R., & Altschuler, S. (1994). Brain stem localization of rodent esophageal premotor. *Gastroenterology*, 107(3), 728–737.
- Bass, A. H. (2014). Central pattern generator for vocalization: Is there a vertebrate morphotype? *Current Opinion in Neurobiology*, 28, 94–100. <https://doi.org/10.1016/j.conb.2014.06.012>
- Bass, A. H., & Remage-healey, L. (2008). Central pattern generators for social vocalization: Androgen-dependent neurophysiological mechanisms. *Hormones and Behavior*, 53, 659–672. <https://doi.org/10.1016/j.yhbeh.2007.12.010>
- Bennett, P. J. G., Maier, E., & Brecht, M. (2019). Involvement of rat posterior prelimbic and cingulate area 2 in vocalization control. *European Journal of Neuroscience*, 50(7), 3164–3180. <https://doi.org/10.1111/ejn.14477>
- Brainard, M. S., & Doupe, A. J. (2013). Translating birdsong: Songbirds as a model for basic and applied medical research. *Annual Review of Neuroscience*, 36(1), 489–517. <https://doi.org/10.1146/annurev-neuro-060909-152826>
- Burkhard, T. T., Westwick, R. R., & Phelps, S. M. (2018). Adiposity signals predict vocal effort in Alston's singing mice. *Proceedings of the Royal Society B: Biological Sciences*, 285(1877), 20180090. <https://doi.org/10.1098/rspb.2018.0090>
- Callaway, E. M. (2008). Transneuronal circuit tracing with neurotropic viruses. *Current Opinion in Neurobiology*, 18(6), 617–623. <https://doi.org/10.1016/j.conb.2009.03.007>
- Campbell, P., Pasch, B., Pino, J. L., Crino, O. L., Phillips, M., & Phelps, S. M. (2010). Geographic variation in the songs of neotropical singing mice: Testing the relative importance of drift and local adaptation. *Evolution; International Journal of Organic Evolution*, 64(7), 1955–1972. <https://doi.org/10.1111/j.1558-5646.2010.00962.x>

- Card, J. P., & Enquist, L. W. (2014). Transneuronal circuit analysis with pseudorabies viruses. *Current Protocols in Neuroscience*, 68, 1.5.1–1.5.39. <https://doi.org/10.1002/0471142301.ns0105s68>
- Van Daele, D. J., & Cassell, M. D. (2010). Multiple forebrain systems converge on motor neurons innervating the thyroarytenoid muscle. *Neuroscience*, 162(2), 501–524. <https://doi.org/10.1016/j.neuroscience.2009.05.005>. Multiple
- Chabout, J., Sarkar, A., Patel, S. R., Radden, T., Dunson, D. B., Fisher, S. E., & Jarvis, E. D. (2016). A Foxp2 mutation implicated in human speech deficits alters sequencing of ultrasonic vocalizations in adult male mice. *Frontiers in Behavioral Neuroscience*, 10, 197. <https://doi.org/10.3389/fnbeh.2016.00197>
- Chen, S., Yang, M., Miselis, R. R., & Aston-Jones, G. (1999). Characterization of transsynaptic tracing with central application of pseudorabies virus. *Brain Research*, 838(1–2), 171–183. [https://doi.org/10.1016/S0006-8993\(99\)01680-7](https://doi.org/10.1016/S0006-8993(99)01680-7)
- Chen, M., Reed, R. R., & Lane, A. P. (2017). Acute inflammation regulates neuroregeneration through the NF- κ B pathway in olfactory epithelium. *Proceedings of the National Academy of Sciences of the United States of America*, 114(30), 8089–8094. <https://doi.org/10.1073/pnas.1620664114>
- Chen, Z., & Wiens, J. J. (2020). The origins of acoustic communication in vertebrates. *Nature Communications*, 11(1), 1–8. <https://doi.org/10.1038/s41467-020-14356-3>
- Chen, J., Markowitz, J. E., Lilascharoen, V., Taylor, S., Sheurpudki, P., Keller, J. A., Jensen, J. R., Lim, B. K., Datta, S. R., & Stowers, L. (2021). Flexible scaling and persistence of social vocal communication. *Nature*, 593(7857), 108–113. <https://doi.org/10.1038/s41586-021-03403-8>
- Connell, L. A. O., & Hofmann, H. A. (2011). The Vertebrate mesolimbic reward system and social behavior network: A comparative synthesis. *Journal of Comparative Neurology*, 3639, 3599–3639. <https://doi.org/10.1002/cne.22735>
- Crino, O. L., Larkin, I., & Phelps, S. M. (2010). Stress coping styles and singing behavior in the short-tailed singing mouse (*Scotinomys teguina*). *Hormones and Behavior*, 58(2), 334–340. <https://doi.org/10.1016/j.yhbeh.2010.02.011>
- Cummings, M. E., & Endler, J. A. (2018). 25 Years of sensory drive: The evidence and its watery bias. *Current Zoology*, 64(4), 471–484. <https://doi.org/10.1093/cz/zoy043>
- Doslíková, B., Tchir, D., McKinty, A., Zhu, X., Marks, D. L., Baracos, V. E., & Colmers, W. F. (2019). Convergent neuronal projections from paraventricular nucleus, parabrachial nucleus, and brainstem onto gastrocnemius muscle, white and brown adipose tissue in male rats. *Journal of Comparative Neurology*, 527(17), 2826–2842. <https://doi.org/10.1002/cne.24710>
- Dujardin, E., & Jürgens, U. (2006). Call type-specific differences in vocalization-related afferents to the periaqueductal gray of squirrel monkeys (*Saimiri sciureus*). *Behavioural Brain Research*, 168(1), 23–36. <https://doi.org/10.1016/j.bbr.2005.10.006>
- Esposito, A., Demeurisse, G., Alberti, B., & Fabbro, F. (1999). Complete mutism after midbrain periaqueductal gray lesion. *NeuroReport*, 10(4), 681–685. <https://doi.org/10.1097/00001756-199903170-00004>
- Falkner, A. L., Wei, D., Song, A., Watsek, L. W., Chen, I., Chen, P., Chen, P., Feng, J. E., & Lin, D. (2020). Hierarchical representations of aggression in a hypothalamic-midbrain circuit. *Neuron*, 106(4), 637–648.e6. <https://doi.org/10.1016/j.neuron.2020.02.014>
- Farley, G. R., Barlow, S. M., & Netsell, R. (1992). Factors influencing neural activity in parabrachial regions during cat vocalizations. *Experimental Brain Research*, 89(2), 341–351. <https://doi.org/10.1007/BF00228250>
- Fay, R. A., & Norgren, R. (1997). Identification of rat brainstem multisynaptic connections to the oral motor nuclei in the rat using pseudorabies virus II. Facial muscle motor systems. *Brain Research Reviews*, 25, 276–290.
- Fee, M. S., Kozhevnikov, A. A., & Hahnloser, R. H. R. (2004). Neural mechanisms of vocal sequence generation in the songbird. *Annals of the New York Academy of Sciences*, 1016, 153–170. <https://doi.org/10.1196/annals.1298.022>
- Fernández-Vargas, M., Tang-Martínez, Z., & Phelps, S. M. (2011). Singing, allogrooming, and allomarking behaviour during inter- and intra-sexual encounters in the Neotropical short-tailed singing mouse (*Scotinomys teguina*). *Behaviour*, 148(8), 945–965. <https://doi.org/10.1163/000579511X584591>
- Foote, S. L., Freedman, R., & Oliver, A. P. (1975). Effects of putative neurotransmitters on neuronal activity in monkey auditory cortex. *Brain Research*, 86(2), 229–242. [https://doi.org/10.1016/0006-8993\(75\)90699-x](https://doi.org/10.1016/0006-8993(75)90699-x)
- Franklin, K. B., & Paxinos, G. (2007). *The mouse atlas in stereotaxic coordinates* (3rd ed.). Elsevier.
- Fusani, L., Barske, J., Day, L. D., Fuxjager, M. J., & Schlinger, B. A. (2014). Physiological control of elaborate male courtship: Female choice for neuromuscular systems. *Neuroscience and Biobehavioral Reviews*, 46(P4), 534–546. <https://doi.org/10.1016/j.neubiorev.2014.07.017>
- Gao, S.-C., Wei, Y.-C., Wang, S.-R., & Xu, X.-H. (2019). Medial preoptic area modulates courtship ultrasonic vocalization in adult male mice. *Neuroscience Bulletin*, 35(4), 697–708. <https://doi.org/10.1007/s12264-019-00365-w>
- Gentner, T. Q., & Margoliash, D. (2006). The neuroethology of vocal communication: Perception and cognition. In A. M. Simmons, R. R. Fay, & A. N. Popper (Eds.), *Acoustic communication* (pp. 324–386). Springer. https://doi.org/10.1007/0-387-22762-8_7
- Giglio, E. M., & Phelps, S. M. (2020). Leptin regulates song effort in Neotropical singing mice (*Scotinomys teguina*). *Animal Behaviour*, 167, 209–219. <https://doi.org/10.1016/j.anbehav.2020.06.022>
- Goodson, J. L. (2005). The vertebrate social behavior network: Evolutionary themes and variations. *Hormones and Behavior*, 48, 11–22. <https://doi.org/10.1016/j.yhbeh.2005.02.003>
- Goodson, J. L., & Bass, A. H. (2000). Forebrain peptides modulate sexually polymorphic vocal circuitry. *Nature*, 403(6771), 769–772. <https://doi.org/10.1038/35001581>
- Goodson, J. L., & Bass, A. H. (2002). Vocal-acoustic circuitry and descending vocal pathways in teleost fish: Convergence with terrestrial vertebrates reveals conserved traits. *Journal of Comparative Neurology*, 448(3), 298–322. <https://doi.org/10.1002/cne.10258>
- Green, D. B., Shackleton, T. M., Grimsley, J. M. S., Zobay, O., Palmer, A. R., & Wallace, M. N. (2018). Communication calls produced by electrical stimulation of four structures in the guinea pig brain. *PLoS One*, 13(3), e0194091. <https://doi.org/10.1371/journal.pone.0194091>
- Greenberg, G. D., Steinman, M. Q., Doig, I. E., Hao, R., & Trainor, B. C. (2015). Effects of social defeat on dopamine neurons in the ventral tegmental area in male and female California mice. *The European journal of neuroscience*, 42(12), 3081–3094. <https://doi.org/10.1111/ejn.13099>
- Gruber-Dujardin, E. (2010). Role of the periaqueductal gray in expressing vocalization. In S. M. Brudzynski (Ed.), *Handbook of mammalian vocalization* (1st ed., pp. 313–328). Elsevier.
- Guyenet, P. G., Koshiya, N., Huangfu, D., Verberne, A. J. M., & Riley, T. A. (1993). Central respiratory control of A5 and A6 pontine noradrenergic neurons. *American Journal of Physiology—Regulatory Integrative and Comparative Physiology*, 264(6), 33–6. <https://doi.org/10.1152/ajpregu.1993.264.6.r1035>
- Hage, S. R. (2010). Localization of the central pattern generator for vocalization. In S. M. Brudzynski (Ed.), *Handbook of mammalian vocalization* (1st ed., pp. 329–337). Elsevier.
- Hage, S. R., & Nieder, A. (2016). Dual neural network model for the evolution of speech and language. *Trends in Neurosciences*, 39(12), 813–829. <https://doi.org/10.1016/j.tins.2016.10.006>
- Hall, I. C., Ballagh, I. H., & Kelley, D. B. (2013). The *Xenopus* amygdala mediates socially appropriate vocal communication signals. *Journal of Neuroscience*, 33(36), 14534–14548. <https://doi.org/10.1523/JNEUROSCI.1190-13.2013>

- Hamed, A., & Boguszewski, P. M. (2018). Effects of morphine and other opioid ligands on emission of ultrasonic vocalizations in rats. In S. M. Brudzynski (Ed.), *Handbook of behavioral neuroscience* (1st ed., vol. 25, pp. 327–334). Elsevier. <https://doi.org/10.1016/B978-0-12-809600-0.00031-7>
- Herbert, H., Moga, M. M., & Saper, C. B. (1990). Connections of the peribrachial nucleus with the nucleus of the solitary tract and the medullary reticular formation in the rat. *The Journal of Comparative Neurology*, 293(4), 540–580. <https://doi.org/10.1002/cne.902930404>
- Hernandez-Miranda, L. R., Ruffault, P. L., Bouvier, J. C., Murray, A. J., Morin-Surun, M. P., Zampieri, N., Cholewa-Waclaw, J. B., Ey, E., Brunet, J.-F., Champagnat, J., Fortin, G., & Birchmeier, C. (2017). Genetic identification of a hindbrain nucleus essential for innate vocalization. *Proceedings of the National Academy of Sciences of the United States of America*, 114(30), 8095–8100. <https://doi.org/10.1073/pnas.1702893114>
- Hettigoda, N. S., Fong, A. Y., Badoer, E., McKinley, M. J., Oldfield, B. J., & Allen, A. M. (2015). Identification of CNS neurons with polysynaptic connections to both the sympathetic and parasympathetic innervation of the submandibular gland. *Brain Structure and Function*, 220(4), 2103–2120. <https://doi.org/10.1007/s00429-014-0781-1>
- Hilaire, G., Viemari, J.-C., Coulon, P., Simonneau, M., & Bévingut, M. (2004). Modulation of the respiratory rhythm generator by the pontine noradrenergic A5 and A6 groups in rodents. *Respiratory Physiology & Neurobiology*, 143(2–3), 187–197. <https://doi.org/10.1016/j.resp.2004.04.016>
- Hisa, Y. (2016). Neuroanatomy and neurophysiology of the larynx. *Neuroanatomy and neurophysiology of the larynx* (pp. 1–123). Springer. <https://doi.org/10.1007/978-4-431-55750-0>
- Hisa, Y., Sato, F., Fukui, K., Ibata, Y., & Mizukoshi, O. (1984). Nucleus ambiguus motoneurons innervating the canine intrinsic laryngeal muscles by the fluorescent labeling technique. *Experimental Neurology*, 84, 441–449.
- Hogue, I. B., Card, J. P., Rinaman, L., Staniszewska Goracznik, H., & Enquist, L. W. (2018). Characterization of the neuroinvasive profile of a pseudorabies virus recombinant expressing the mTurquoise2 reporter in single and multiple injection experiments. *Journal of Neuroscience Methods*, 308(August), 228–239. <https://doi.org/10.1016/j.jneumeth.2018.08.004>
- Hooper, E. T., & Carleton, M. D. M. (1976). *Reproduction, growth and development in two contiguously allopatric rodent species, genus Scotinomys*. <http://deepblue.lib.umich.edu/handle/2027.42/56395>
- Iv, E. S., Cheng, S., Takatoh, J., Han, B., & Wang, F. (2014). Monosynaptic premotor circuit tracing reveals neural substrates for oro-motor coordination. *eLife*, 3, 1–23. <https://doi.org/10.7554/eLife.02511>
- Jovanovic, K., Pastor, A. M., & O'Donovan, M. J. (2010). The use of PRV-bartha to define premotor inputs to lumbar motoneurons in the neonatal spinal cord of the mouse. *PLoS One*, 5(7), e11743. <https://doi.org/10.1371/journal.pone.0011743>
- Jürgens, U. (1982). Amygdalar vocalization pathways in the squirrel monkey. *Brain Research*, 241(2), 189–196. [https://doi.org/10.1016/0006-8993\(82\)91055-1](https://doi.org/10.1016/0006-8993(82)91055-1)
- Jürgens, U. (1994). The role of the periaqueductal grey in vocal behaviour. *Behavioural Brain Research*, 62(2), 107–117. [https://doi.org/10.1016/0166-4328\(94\)90017-5](https://doi.org/10.1016/0166-4328(94)90017-5)
- Jürgens, U. (2009). The neural control of vocalization in mammals: A review. *Journal of Voice: Official Journal of the Voice Foundation*, 23(1), 1–10. <https://doi.org/10.1016/j.jvoice.2007.07.005>
- Jürgens, U., Maurus, M., Ploog, D., & Winter, P. (1967). Vocalization in the squirrel monkey (*Saimiri sciureus*) elicited by brain stimulation. *Experimental Brain Research*, 4(2), 114–117. <https://doi.org/10.1007/BF00240356>
- Jürgens, U., & Ploog, D. (1970). Cerebral representation of vocalization in the squirrel monkey. *Experimental Brain Research*, 10(5), 532–554. <https://doi.org/10.1007/BF00234269>
- Jürgens, U. (2002). Neural pathways underlying vocal control. *Neuroscience and Biobehavioral Reviews*, 26(2), 235–258. [https://doi.org/10.1016/S0149-7634\(01\)00068-9](https://doi.org/10.1016/S0149-7634(01)00068-9)
- Kang, T. C., Lee, B. H., Seo, J., Song, S. H., Kim, J. S., Won, M. H., Lee, I. S., & Lee, H. S. (1999). The nuclei innervating digastric muscle do not project to the hypoglossal nucleus in the rat. *Anatomia, Histologia, Embryologia*, 28(1), 39–40. <https://doi.org/10.1046/j.1439-0264.1999.00159.x>
- Kelley, D. B., Ballagh, I. H., Barkan, C. L., Bendesky, A., Elliott, T. M., Evans, B. J., Hall, I. C., Kwon, Y. M., Kwong-Brown, U., Leininger, E. C., Perez, E. C., Rhodes, H. J., Villain, A., Yamaguchi, A., & Zornik, E. (2020). Generation, coordination, and evolution of neural circuits for vocal communication. *Journal of Neuroscience*, 40(1), 22–36. <https://doi.org/10.1523/JNEUROSCI.0736-19.2019>
- Kemplay, S., & Cavanagh, J. B. (1983). Bilateral innervation of the anterior digastric muscle by trigeminal motor neurons. *Journal of Anatomy*, 136(Pt 2), 417–423. Retrieved from <https://pubmed.ncbi.nlm.nih.gov/6853354>
- Kingsbury, M. A., Kelly, A. M., Schrock, S. E., & Goodson, J. L. (2011). Mammal-like organization of the avian midbrain central gray and a reappraisal of the intercollicular nucleus. *PLoS One*, 6(6), e20720. <https://doi.org/10.1371/journal.pone.0020720>
- Kittelberger, J. M., & Bass, A. H. (2013). Vocal-motor and auditory connectivity of the midbrain periaqueductal gray in a teleost fish. *Journal of Comparative Neurology*, 521(4), 791–812. <https://doi.org/10.1002/cne.23202>
- Kobiler, O., Lipman, Y., Therkelsen, K., Daubechies, I., & Enquist, L. W. (2010). Herpesviruses carrying a brainbow cassette reveal replication and expression of limited numbers of incoming genomes. *Nature Communications*, 1(1), 146. <https://doi.org/10.1038/ncomms1145>
- Koblinger, K., Füzesi, T., Ejdrygiewicz, J., Krajacic, A., Bains, J. S., & Whelan, P. J. (2014). Characterization of A11 neurons projecting to the spinal cord of mice. *PLoS One*, 9(10), e109636. <https://doi.org/10.1371/journal.pone.0109636>
- Komiyama, T., Sato, T. R., O'Connor, D. H., Zhang, Y.-X., Huber, D., Hooks, B. M., Gabbito, M., & Svoboda, K. (2010). Learning-related fine-scale specificity imaged in motor cortex circuits of behaving mice. *Nature*, 464(7292), 1182–1186. <https://doi.org/10.1038/nature08897>
- Larsen, P. J., Hay-Schmidt, A., & Mikkelsen, J. D. (1994). Efferent connections from the lateral hypothalamic region and the lateral preoptic area to the hypothalamic paraventricular nucleus of the rat. *The Journal of Comparative Neurology*, 342(2), 299–319. <https://doi.org/10.1002/cne.903420211>
- Lein, E. S., Hawrylycz, M. J., Ao, N., Ayres, M., Bensinger, A., Bernard, A., Boe, A. F., Boguski, M. S., Brockway, K. S., Byrnes, E. J., Chen, L., Chen, T.-M., Chin, M. C., Chong, J., Crook, B. E., Czaplinska, A., Dang, C. N., Datta, S., ... Jones, A. R. (2007). Genome-wide atlas of gene expression in the adult mouse brain. *Nature*, 445(7124), 168–176. <https://doi.org/10.1038/nature05453>
- Ma, J., & Kanwal, J. S. (2014). Stimulation of the basal and central amygdala in the mustached bat triggers echolocation and agonistic vocalizations within multimodal output. *Frontiers in Physiology*, 5. <https://doi.org/10.3389/fphys.2014.00055>
- Manteuffel, G., Schön, P. C., Döpjan, S., Tuchscherer, A., & Bellmann, O. (2007). Acetylcholine injection into the amygdala elicits vocalization in domestic pigs (*Sus scrofa*). *Behavioural Brain Research*, 178(1), 177–180. <https://doi.org/10.1016/j.bbr.2006.12.007>
- Martins, A. R. O., & Froemke, R. C. (2015). Coordinated forms of noradrenergic plasticity in the locus coeruleus and primary auditory cortex. *Nature Neuroscience*, 18(10), 1483–1492. <https://doi.org/10.1038/nn.4090>
- Mercer Lindsay, N., Knutsen, P. M., Lozada, A. F., Gibbs, D., Karten, H. J., & Kleinfeld, D. (2019). Orofacial movements involve parallel corticobulbar projections from motor cortex to trigeminal premotor nuclei. *Neuron*, 104(4), 765–780.e3. <https://doi.org/10.1016/j.neuron.2019.08.032>
- Michael, V., Goffinet, J., Pearson, J., Wang, F., Tschida, K., & Mooney, R. (2020). Circuit and synaptic organization of forebrain-to-midbrain pathways that promote and suppress vocalization. *eLife*, 9, e63493. <https://doi.org/10.7554/eLife.63493>
- Miller, J. R., & Engstrom, M. D. (2007). Vocal stereotypy and singing behavior in baiomyine mice. *Journal of Mammalogy*, 88, 1447–1465. <https://doi.org/10.1644/06-MAMM-A-386R.1>

- Moore, J. D., Kleinfeld, D., & Wang, F. (2014). How the brainstem controls orofacial behaviors comprised of rhythmic actions. *Trends in Neurosciences*, 37(7), 370–380. <https://doi.org/10.1016/j.tins.2014.05.001>
- Morton, E. S. (2017). *Animal vocal communication: Assessment and management roles*. Cambridge University Press.
- Morton, G. J., Cummings, D. E., Baskin, D. G., Barsh, G. S., & Schwartz, M. W. (2006). Central nervous system control of food intake and body weight. *Nature*, 443(7109), 289–295. <https://doi.org/10.1038/nature05026>
- Nevue, A. A., Felix 2nd, R. A., & Portfors, C. V. (2016). Dopaminergic projections of the subparafascicular thalamic nucleus to the auditory brainstem. *Hearing Research*, 341, 202–209. <https://doi.org/10.1016/j.heares.2016.09.001>
- Newman, S. W. (1999). The medial extended amygdala in male reproductive behavior. A node in the mammalian social behavior network. *Annals of the New York Academy of Sciences*, 877, 242–257. <https://doi.org/10.1111/j.1749-6632.1999.tb09271.x>
- Nieder, A., & Mooney, R. (2020). The neurobiology of innate, volitional and learned vocalizations in mammals and birds. *Philosophical Transactions of the Royal Society B: Biological Sciences*, 375(1789), 20190054. <https://doi.org/10.1098/rstb.2019.0054>
- Núñez-Abades, P. A., Portillo, F., & Páraso, R. (1990). Characterisation of afferent projections to the nucleus ambiguus of the rat by means of fluorescent double labelling. *Journal of Anatomy*, 172, 1–15.
- Okobi, D. E., Banerjee, A., Matheson, A. M. M., Phelps, S. M., & Long, M. A. (2019). Motor cortical control of vocal interaction in neotropical singing mice. *Science*, 363(6430), 983–988. <https://doi.org/10.1126/science.aau9480>
- Okobi, D. E. (2016). A cortical locus modulates vocal motor sequences in Alston's singing mouse (*Scotinomys teguina*) by Daniel Ebele Okobi, Jr. [Dissertation submitted in partial fulfillment of the requirements for the degree of Doctor of Philosophy Department of Basic].
- Pasch, B., Bolker, B. M., & Phelps, S. M. (2013). Interspecific dominance via vocal interactions mediates altitudinal zonation in neotropical singing mice. *The American Naturalist*, 182(5), E161–E173. <https://doi.org/10.1086/673263>
- Pasch, B., George, A. S., Campbell, P., & Phelps, S. M. (2011a). Androgen-dependent male vocal performance influences female preference in neotropical singing mice. *Animal Behaviour*, 82(2), 177–183. <https://doi.org/10.1016/j.anbehav.2011.04.018>
- Pasch, B., George, A. S., Hamlin, H. J., Jr, L. J. G., & Phelps, S. M. (2011). Hormones and behavior androgens modulate song effort and aggression in neotropical singing mice. *Hormones and Behavior*, 59(1), 90–97. <https://doi.org/10.1016/j.yhbeh.2010.10.011>
- Pérez, C. A., Stanley, S. A., Wysocki, R. W., Havranova, J., Ahrens-Nicklas, R., Onyimba, F., & Friedman, J. M. (2011). Molecular annotation of integrative feeding neural circuits. *Cell Metabolism*, 13(2), 222–232. <https://doi.org/10.1016/j.cmet.2010.12.013>
- Pickard, G. E., Smeraski, C. A., Tomlinson, C. C., Banfield, B. W., Kaufman, J., Wilcox, C. L., Enquist, L. W., & Sollars, P. J. (2002). Intravitreal injection of the attenuated pseudorabies virus PRV Bartha results in infection of the hamster suprachiasmatic nucleus only by retrograde transsynaptic transport via autonomic circuits. *The Journal of neuroscience: the official journal of the Society for Neuroscience*, 22(7), 2701–2710. <https://doi.org/10.1523/JNEUROSCI.22-07-02701.2002>
- Prins, G. S., Birch, L., & Greene, G. L. (1991). Androgen receptor localization in different cell types of the adult rat prostate. *Endocrinology*, 129(6), 3187–3199. <https://doi.org/10.1210/endo-129-6-3187>
- Remage-Healey, L., Maidment, N. T., & Schlinger, B. A. (2008). Forebrain steroid levels fluctuate rapidly during social interactions. *Nature Neuroscience*, 11(11), 1327–1334. <https://doi.org/10.1038/nn.2200>
- Rhodes, H. J., Yu, H. J., & Yamaguchi, A. (2007). Xenopus vocalizations are controlled by a sexually differentiated hindbrain central pattern generator. *The Journal of Neuroscience: The Official Journal of the Society for Neuroscience*, 27(6), 1485–1497. <https://doi.org/10.1523/JNEUROSCI.4720-06.2007>
- Riede, T. (2013). Stereotypic laryngeal and respiratory motor patterns generate different call types in rat ultrasound vocalization. *Journal of Experimental Zoology. Part A, Ecological Genetics and Physiology*, 319(4), 213–224. <https://doi.org/10.1002/jez.1785>
- Riede, T., & Pasch, B. (2020). Pygmy mouse songs reveal anatomical innovations underlying acoustic signal elaboration in rodents. *The Journal of Experimental Biology*, 223(12), jeb223925. <https://doi.org/10.1242/jeb.223925>
- Robinson, B. W. (1967). Vocalization evoked from forebrain in *Macaca mulatta*. *Physiology & Behavior*, 2(4), 345–354. [https://doi.org/10.1016/0031-9384\(67\)90050-9](https://doi.org/10.1016/0031-9384(67)90050-9)
- Sakata, J. T., & Yazaki-Sugiyama, Y. (2020). Neural circuits underlying vocal learning in songbirds. In J. T. Sakata, S. C. Woolley, R. R. Fay, & A. N. Popper (Eds.), *The neuroethology of birdsong* (pp. 29–63). Springer. https://doi.org/10.1007/978-3-030-34683-6_2
- Saleeba, C., Dempsey, B., Le, S., Goodchild, A., & McMullan, S. (2019). A student's guide to neural circuit tracing. *Frontiers in Neuroscience*, 13, 897. <https://www.frontiersin.org/article/10.3389/fnins.2019.00897>
- Samuels, E. R., & Szabadi, E. (2008). Functional neuroanatomy of the noradrenergic locus coeruleus: Its roles in the regulation of arousal and autonomic function part I: Principles of functional organisation. *Current Neuropharmacology*, 6(3), 235–253. <https://doi.org/10.2174/157015908785777229>
- Saper, C. B., & Loewy, A. D. (1980). Efferent connections of the parabrachial nucleus in the rat. *Brain Research*, 197(2), 291–317. [https://doi.org/10.1016/0006-8993\(80\)91117-8](https://doi.org/10.1016/0006-8993(80)91117-8)
- Sara, S. J. (2009). The locus coeruleus and noradrenergic modulation of cognition. *Nature Reviews Neuroscience*, 10(3), 211–223. <https://doi.org/10.1038/nrn2573>
- Saravanan, V., Hoffmann, L. A., Jacob, A. L., Berman, G. J., & Sober, S. J. (2019). Dopamine depletion affects vocal acoustics and disrupts sensorimotor adaptation in songbirds. *eNeuro*, 6(3). <https://doi.org/10.1523/ENEURO.0190-19.2019>
- Schlinger, B. A., Paul, K., & Monks, D. A. (2018). Muscle, a conduit to brain for hormonal control of behavior. *Hormones and Behavior*, 105(August), 58–65. <https://doi.org/10.1016/j.yhbeh.2018.07.002>
- Schmidt, R. S. (1968). Preoptic activation of frog mating behavior. *Behaviour*, 30(2/3), 239–257. <http://www.jstor.org/stable/4533213>
- Schneider, N. Y., Chaudy, S., Epstein, A. L., et al. (2020). Centrifugal projections to the main olfactory bulb revealed by transsynaptic retrograde tracing in mice. *J Comp Neurol*. 528, 1805–1819. <https://doi.org/10.1002/cne.24846>
- Schwartz, C. P., & Smotherman, M. S. (2011). Mapping vocalization-related immediate early gene expression in echolocating bats. *Behavioural Brain Research*, 224(2), 358–368. <https://doi.org/10.1016/j.bbr.2011.06.023>
- Simonyan, K. (2014). The laryngeal motor cortex: Its organization and connectivity. *Current Opinion in Neurobiology*, 28, 15–21. <https://doi.org/10.1016/j.conb.2014.05.006>
- Simonyan, K., Horwitz, B., & Jarvis, E. D. (2012). Dopamine regulation of human speech and bird song: A critical review. *Brain and Language*, 122(3), 142–150. <https://doi.org/10.1016/j.bandl.2011.12.009>
- Smotherman, M., Schwartz, C., & Metzner, W. (2010). Vocal-respiratory interactions in the parabrachial nucleus. In S. M. Brudzynski (Ed.), *Handbook of mammalian vocalization* (1st ed., pp. 383–392). Elsevier.
- Stanley, S., Pinto, S., Segal, J., Pérez, C. A., Viale, A., DeFalco, J., Cai, X., Heisler, L. K., & Friedman, J. M. (2010). Identification of neuronal subpopulations that project from hypothalamus to both liver and adipose tissue polysynaptically. *Proceedings of the National Academy of Sciences of the United States of America*, 107(15), 7024–7029. <https://doi.org/10.1073/pnas.1002790107>
- Steppan, S. J., & Schenk, J. J. (2017). Muroid rodent phylogenetics: 900-species tree reveals increasing diversification rates. *PLoS One*, 12(8), e0183070. <https://doi.org/10.1371/journal.pone.0183070>

- Stuber, G. D., & Wise, R. A. (2016). Lateral hypothalamic circuits for feeding and reward. *Nature Neuroscience*, 19(2), 198–205. <https://doi.org/10.1038/nn.4220>
- Suthers, R. A., Fitch, W. T., Fay, R. R., & Popper, A. N. (2004). Vertebrate sound production and acoustic communication. In R. Fay & A. N. Popper (Eds.), *The senses of fish* (pp. 19–49). Springer Handbook of Auditory Research. <https://doi.org/10.1007/978-3-319-27721-9>
- Szabadi, E. (2013). Functional neuroanatomy of the central noradrenergic system. *Journal of Psychopharmacology*, 27(8), 659–693. <https://doi.org/10.1177/0269881113490326>
- Tschida, K., Michael, V., Takatoh, J., Han, B. X., Zhao, S., Sakurai, K., Mooney, R., & Wang, F. (2019). A specialized neural circuit gates social vocalizations in the mouse. *Neuron*, 103(3), 459–472.e4. <https://doi.org/10.1016/j.neuron.2019.05.025>
- Ugolini, G. (2010). Advances in viral transneuronal tracing. *Journal of neuroscience methods*, 194(1), 2–20. <https://doi.org/10.1016/j.jneumeth.2009.12.001>
- Waldbaum, S., Hadziefendic, S., Erokwu, B., Zaidi, S. I. A., & Haxhiu, M. A. (2001). CNS innervation of posterior cricoarytenoid muscles: A transneuronal labeling study. *Respiration Physiology*, 126(2), 113–125. [https://doi.org/10.1016/S0034-5687\(01\)00200-6](https://doi.org/10.1016/S0034-5687(01)00200-6)
- Wee, N. K. Y., Lorenz, M. R., Bekirov, Y., Jacquin, M. F., & Scheller, E. L. (2019). Shared autonomic pathways connect bone marrow and peripheral adipose tissues across the central neuraxis. *Frontiers in Endocrinology*, 10(Sep), 1–16. <https://doi.org/10.3389/fendo.2019.00668>
- Wei, Y. C., Wang, S. R., Jiao, Z. L., Zhang, W., Lin, J. K., Li, X. Y., Li, S. S., Zhang, X., & Xu, X. H. (2018). Medial preoptic area in mice is capable of mediating sexually dimorphic behaviors regardless of gender. *Nature Communications*, 9(1), 279. <https://doi.org/10.1038/s41467-017-02648-0>
- Wiedmann, N. M., Stefanidis, A., & Oldfield, B. J. (2017). Characterization of the central neural projections to brown, white, and beige adipose tissue. *FASEB Journal*, 31(11), 4879–4890. <https://doi.org/10.1096/fj.201700433R>
- Yamaguchi, A., & Kelley, D. B. (2003). Hormonal Mechanisms in Acoustic Communication BT - Acoustic Communication (A. M. Simmons, R. R. Fay, & A. N. Popper, eds.). https://doi.org/10.1007/0-387-22762-8_6
- Yao, J., Zhang, Q., Liao, X., Li, Q., Liang, S., Li, X., ... Chen, X. (2018). A corticopontine circuit for initiation of urination. *Nature Neuroscience*, 21(11), 1541–1550. <https://doi.org/10.1038/s41593-018-0256-4>
- Zhang, Y. S., & Ghazanfar, A. A. (2020). A hierarchy of autonomous systems for vocal production. *Trends in Neurosciences*, 43(2), 115–126. <https://doi.org/10.1016/j.tins.2019.12.006>
- Zheng, D.-J., Singh, A., & Phelps, S. M. (2021). Conservation and dimorphism in androgen receptor distribution in Alston's singing mouse (*Scotinomys teguina*). *Journal of Comparative Neurology*, 529(10), 2539–2557. <https://doi.org/10.1002/cne.25108>

How to cite this article: Zheng, D.-J., Okobi, D. E., Shu, R., Agrawal, R., Smith, S. K., Long, M. A., & Phelps, S. M. (2022). Mapping the vocal circuitry of Alston's singing mouse with pseudorabies virus. *Journal of Comparative Neurology*, 530, 2075–2099. <https://doi.org/10.1002/cne.25321>